THREE-DIMENSIONAL FINITE ELEMENT MODELING OF PACINIAN CORPUSCLE

by

Serkan Yelke

B.S., Mechanical Engineering, ITU, 2004

Submitted to the Institute of Biomedical Engineering
in partial fulfillment of the requirements
for the degree of
Master of Science
in
Biomedical Engineering

Boğaziçi University
February 2008

ACKNOWLEDGMENTS

I would like to thank to my family, my friends and instructors who gave the strength and inspiration to finish this study.

ABSTRACT

THREE-DIMENSIONAL FINITE ELEMENT MODELING OF PACINIAN CORPUSCLE

Understanding the mechanics of Pacinian corpuscle (PC) is a fundamental necessity in order to contribute to tactile sense studies. It is proposed that the geometry of PC may have impact on its mechanics. A three-dimensional ovoid shape PC model was developed using the finite element method. The viscoelastic coefficients were included to involve time dependent material properties and to observe whether the band-pass filtering characteristics of PC obtained from neurophysiological data may be observed in the finite element model of PC or not. Static and dynamic stimulations were given to the model as inputs to mimic experiments. Data from both model and experiments were compared and it was concluded that geometry has no determining effect on the mechanics of PC. Besides, viscoelastic property, alone, was not enough to comprehend the underlying reason of band-pass filtering characteristics of PC. Homogeneous structure may not be the only answer to the mismatch of the results since the filtering property was not observed in experimental studies. If the homogeneous structure of the model is developed to a multilayered structure, more reliable results would have been obtained which needs to be tested in new studies.

Keywords: Pacinian corpuscle, finite element method, viscoelasticity, band-pass filter, mechanoreceptor.

ÖZET

ÜÇ BOYUTLU PAÇİNİ CİSİMCİĞİNİN SONLU ELEMANLAR MODELİ

Dokunma duyusunun üzerine yapılan çalışmaların büyük bir bölümünü Pacini cisimciği (PC) ile ilgili olan çalışmalar kapsar. Bu nedenle, PC mekaniğini bilmek oldukça büyük bir önem arz etmektedir. Bu noktadan yola çıkarak daha önce yapılmamış olan üç boyutlu beyzi şekilli bir PC modeli sonlu elemanlar metodu kullanılarak oluşturuldu. Oluşturulan bu modele viskoelastik materyal özellikleri girilmiştir ancak PC'nin yapısı homojen kabul edilmiştir. Böylece daha önce sorgulanmamış olan üç boyutlu geometrinin PC mekaniği üzerindeki etkisi anlaşılabilecek, viskoelastik parametrelerin cisimde daha önce gözlemlenen bant-geçirir filtreleme özelliğini ortaya çıkarıp çıkaramayacağı anlaşılacaktır. Deneysel çalışmaların sonuçlarını modelle karşılaştırabilmek ve yorumlayabilmek amacıyla deneysel çalışmalarda kullanılan mekanik uyarıların aynısı modele de uygulanmıştır. Uygulanan statik uyarıların sonucunda PC'nin üç boyutlu geometrisinin mekaniğinde belirleyici etkisi olmadığı ortaya çıktı. Ayrıca sinirden alınan ölçümlerde sadece çok küçük genlikler için böyle bir filtrelemeden söz edilebilirken, deneysel çalışmalarda teknik yetersizlikler nedeniyle aynı genlikler test edilememiştir. Önerilen modelin sonuçlarında, uyarı genliğinden bağımsız olarak, filtreleme özelliğinin görülmemesi bu özelliğin temelini oluşturan sebep hakkında çeşitli görüşlere yol açmaktadır. Çok katmanlı olarak geliştirilmiş daha karmaşık yapıdaki bir PC modeli bu görüşlere net bir yanıt verebilir.

Anahtar Sözcükler: Pacini cisimciği, sonlu elemanlar yöntemi, viskoelastisite, band geçirir filtre, mekanoreseptör.

TABLE OF CONTENTS

ACKNOWLEDGMENTS . . . iii
ABSTRACT . . . iv
ÖZET . . . v
LIST OF FIGURES . . . viii
LIST OF TABLES . . . xii
LIST OF SYMBOLS . . . xiii
LIST OF ABBREVIATIONS . . . xiv
1. INTRODUCTION . . . 1
2. THEORETICAL BACKGROUND . . . 2
2.1 Pacinian Corpuscle (PC) . . . 2
2.1.1 Structure . . . 4
2.1.1.1 Outer core and external capsule . . . 7
2.1.1.2 Inner core . . . 9
2.1.1.3 Intermediate layer . . . 12
2.1.1.4 Neurite . . . 13
2.1.2 Function . . . 17
2.1.2.1 Receptor and action potentials . . . 20
2.2 Previous PC Models . . . 22
2.3 Finite Element Method (FEM) . . . 24
3. METHODS . . . 31
3.1 Previous Experimental Assessment . . . 31
3.2 Model . . . 32
3.2.1 Test Model . . . 33
3.2.1.1 The Maxwell model . . . 34
3.2.2 Actual PC Model . . . 39
3.2.3 Mechanical Stimulations . . . 44
4. RESULTS . . . 47
4.1 Test Model . . . 47
4.2 Actual model . . . 48

4.2.1 Static Indentation Simulation 48
4.2.2 Dynamic Indentation Simulation 49
5. DISCUSSION AND CONCLUSION 53
5.1 Test Model 53
5.2 Actual Model 55
5.2.1 Static Indentation Simulation 55
5.2.2 Sinusoidal Indentation Simulation 57
5.3 Future Work 61
APPENDIX A. ENGINEERING APPLICATIONS OF THE FEM 62
REFERENCES 65

LIST OF FIGURES

Figure 2.1	PCs are found in clusters [41].	3
Figure 2.2	A PC with clear morphology view in ovoid shape under 80 x magnifications [41].	5
Figure 2.3	A cross-sectional view of PC [Adopted from http://www.scf-online.com/english/26_e/frontpage26_e.htm].	6
Figure 2.4	Schematic illustration of a PC [41].	7
Figure 2.5	Electron micrograph view of a transverse section through the terminal neurite region of a PC, where C is cleft; IC is hemilamellae of inner core; N is elliptical shaped neurite; NI is nucleus of an inner core cell; NO is nucleus of an outer core cell and OC is outer core, and magnified 4000 times [41].	9
Figure 2.6	Electron micrograph view of a transverse section through the terminal neurite region of a PC, where IC is inner core; OC is outer core; IL is intermediate layer; N is neurite and C is cleft, and magnified 9000 times [41].	13
Figure 2.7	Electron micrograph view of a transverse section through the terminal neurite region of a PC with multiple branches of the innervating neurite, which is magnified 6400 times. The separate inner core regions surround the individual neurite processes (N) which have finger-like projection or filopodia (F) projecting into the clefts formed by the gaps separating the inner core hemilamellae [41].	15
Figure 2.8	Electron micrograph view of a transverse section through the terminal neurite region of a PC magnified 19000 times, with various cellular inclusions within the elliptically shaped neurite. In the figure M is mitochondria; NF is neurofilaments; MT is microtubules and V is vescicles. A filopodia (F) projecting into the clefts (C) is formed by the hemilamellae of the inner core [41].	16

Figure 2.9 Electron micrograph views of a transverse section through the terminal neurite region of a PC, which are magnified 10000 (upper micrographs) and 11400 (lower micrograph) times. It can be seen that a filopodium (F) is projecting from the neurite into the cleft region (CF) [41]. 18

Figure 2.10 Electron micrograph view of a transverse section through the ultraterminal region of a PC where N is neurite; L is lamellae and n is nuclei of lamellae cells [41]. 19

Figure 2.11 Signal averaged RPs in response to a 150 Hz sinusoidal stimulus whose amplitude is increased from A to D. The APs are eliminated [41]. 21

Figure 2.12 Polygons are used to calculate the circumference of the circles for the fact that circles are also polygons with infinite number of sides. 26

Figure 2.13 Physical FEM process in block diagram [Adopted from http://www.colorado.edu/engineering/CAS/courses.d/IFEM.d/ IFEM.Ch01.d/IFEM.Ch01.pdf]. 28

Figure 3.1 The camera is placed perpendicular to the stimulus direction unlike previous studies [109]. 32

Figure 3.2 Physiological data is collected from the nerve after the mechanical stimulation of the PC [Adopted from http://www.psych.umn.edu/courses/fall05/burkhardtd/psy3031/images/pacinian.jpg]. 33

Figure 3.3 The test model. 34

Figure 3.4 The Maxwell model [Adopted from http://en.wikipedia.org/wiki/Maxwell_material]. 35

Figure 3.5 The illustration of the experiment in front view. 40

Figure 3.6 The illustration of the experiment in upper right corner view. 41

Figure 3.7 A quarter of PC generated in SolidWorks view. It was generated in such a way that any error at the location of the keypoint is not faced. 42

Figure 3.8 Quarter of PC model generated standing on the rigid plate. 44

Figure 3.9	The contacting element is placed 5 μm above from the contacting point initially.	45
Figure 3.10	The contactor (arranged parallel to the rigid plate) and the PC model.	45
Figure 4.1	The amplitude versus frequency plot (Data from Table 4.1).	48
Figure 4.2	Results of finite element model simulation. Each line is formed from the results of different indentation values. Data are collected from 20 equally separated nodes on the stimulation axis [153].	49
Figure 4.3	Results of Loewenstein and Skalak's model [2] and the performed experiments [153].	50
Figure 4.4	Displacement values of center node and the node 125 μm below from the initial contacting node at the corresponding frequencies [153].	50
Figure 4.5	Stress values of center node and the node 125 μm below from the initial contacting node of finite element model at the corresponding frequencies [153].	51
Figure 4.6	Displacement values collected from the node 125 μm below the initial contacting node of finite element model and 100 μm below the same node of the PC in the experiments [153].	52
Figure 5.1	Characteristics of a high pass filter. Signals below a certain frequency value can not pass through the filter while higher ones can [Adopted from http://www.roland.com/products/en/_support/faq.cfm?iCncd=1076&FAQ=EN06-11040&dsp=1&ln=en&prd = SH201].	54
Figure 5.2	The cut-off point which gives the cut-off frequency in the characteristic high-pass filter curve [Adopted from http://www.making-music.com/eq-and-filters_3.html].	54
Figure 5.3	In Hubbard's study [109] two flats were used to compress the PC in between and the plates were attached from one side so they had an angle between [109].	57

Figure 5.4 The diagram of the apparatus for recording during and after stimulation [109]. 58

Figure 5.5 The static displacements as a function of the indentation amplitude [153]. Previous data set [109] results with filled circles can be fitted by a parabolic curve, but the current experimental data with triangles and diamonds are linear. Each new experimental curve is derived from different depths. The numbers above the R^2 values indicate the locations of the lamella as the ratios of the radius of the chosen lamella to the radius of the capsule, in Hubbard's [109] reference frame, which has the neurite axis going through the origin. 58

Figure 5.6 The curve was fit through the data by eye and indicates average frequency characteristics for two AP response criteria [41]. 59

Figure 5.7 The tuning curves were obtained using the criterion of the minimum amplitude produce one spike per cycle for a capsulated and a decapsulated PC [4]. The experimental results were taken from a previous study [26, 27]. 60

LIST OF TABLES

Table 2.1 Typical parameter values for mesenteric PCs [17, 71, 72, 92, 125] 11

Table 4.1 Results of the test model simulation. The results are represented in units. 47

LIST OF SYMBOLS

mm	Millimeter
mg	Milligram
meq	Milliequivalent
l	Liter
nm	Nanometer
msec	Millisecond
$S^{(l)}$	Lower bound of circumstance
$S^{(u)}$	Upper bound of circumstance
$\mathbf{K}$	Stiffness matrix
$\mathbf{P}$	Load vector
E	Young's modulus
G	Shear modulus
f	Frequency
g	Gram
cm	Centimeter
μm	Micrometer
$\mathbf{\Phi}$	Nodal displacement
σ	Stress
ε	Strain
η	Material viscosity coefficient
α	Material relaxation coefficient
τ	Characteristic relaxation time

LIST OF ABBREVIATIONS

PC	Pacinian Corpuscle
HH	Hodgkin-Huxley Cable Model
FEM	Finite Element Method
CCD	Charge-Coupled Device
USA	United States of America
NY	New York
VHS	Video Home System
GUI	Graphical User Interface
Hz	Hertz
dB	Decibel

1. INTRODUCTION

This study focuses on one of the most important mechanoreceptors of the body referred to as the Pacinian Corpuscle (PC) [1]. A three-dimensional PC model is developed and its response to varying mechanical stimulations is simulated using the finite element method (FEM). One major objective of the study is to understand the mechanics of PC which would be a step to better elucidate some neurophysiological disorders. This is also the basic motivation of the study.

Several studies have been performed to model PC [2–4]. The models were two-dimensional and they did not have viscoelastic material property which is the determining material property in dynamic stimulation simulations. However; there are no existing studies that have attempted to use FEM for three-dimensional modeling of PC. The major contribution of the thesis, hence; is to benefit the advantages of FEM for modeling such an important corpuscle.

The goal of the present study is to construct a three-dimensional viscoelastic finite element PC model. It was aimed at (i) testing whether the geometry has any effect on mechanical excitation and (ii) assessing the possible filtering property of the PC. The former was addressed using static whereas the latter was addressed with dynamic stimulations modeled.

Chapter 1 introduces the thesis. Brief information about theoretical background is given in Chapter 2 which includes the physiology of PC, previous PC models and the FEM. Chapter 3 provides a broad explanation on the design of the experimental protocol and data analysis procedure. Results of the experiments are given in Chapter 4. Finally, a thorough interpretation of results, comparison with previous studies and recommendations for future work are presented in Chapter 5.

2. THEORETICAL BACKGROUND

2.1 Pacinian Corpuscle (PC)

Pacinian corpuscle is one of the most important key elements of the tactile sense. It generates action potential under mechanical stimulation when there is no synapse between the transductive membrane and action-potential generation site. In its core, there is a nerve ending, where the action potential begins [5].

The PCs are generally found at subcutaneous and corium layers of glabrous skin such as hairless part of hands or feet [6, 7]. They are sensitive to mechanically stimulations solely. It has been shown that PCs can not be stimulated by any chemical or thermal stimulators [8–14] and are insensitive to uniform pressure distribution [15, 16]. Beta radiation has also no significant stimulative effect on PCs [17, 18].

The sensitivity of subcutaneous and cutaneous tissues to mechanical stimulations is the key factors that determine the frequency range of sensitivity for PC [11, 14, 19–27]. Human beings sense best between 40-1000 Hz which states the functional significance of PC in tactile perception [23, 28]. Stimulations exceeding these limits are perceived by other mechanoreceptors. In total, there are four psychophysical channels that contribute to the mechanical aspects of the tactile sense. Non - Pacinian mechanoreceptors are Meissner corpuscles, the Merkel - cell neurite complexes and Ruffini corpuscles which are about $1/30$ times sensitive when compared to PC according to the measurements of P channel [23, 25, 29–32]. It has been shown that 0.01 μm of indentation is enough to stimulate PC [26, 27].

PC is widely distributed in human body in the form of clusters (Figure 2.1) [1, 33–41]. About 2000 of them lies in the skin whereas about 700 of them are located only at toes and fingers; and a big portion of them are found to be on fingers [1, 42]. Number of PCs tends to decrease as the age of individual increases which also explains

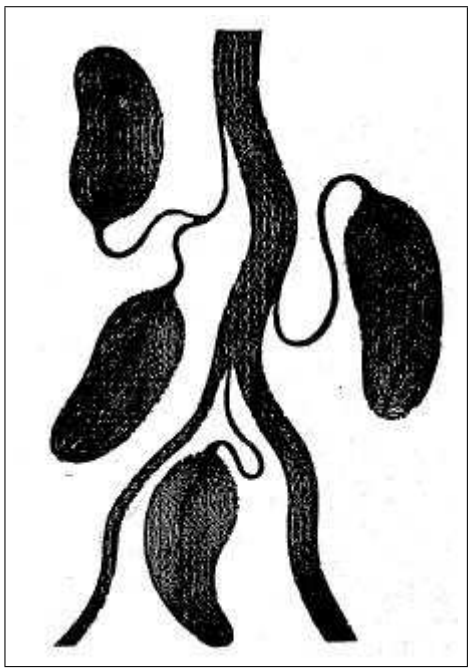

Figure 2.1 PCs are found in clusters [41].

the change in psychophysical P channel with aging [7, 43].

PCs are also found at articular capsules, on tendons, on the fascia or within the muscles, near peripheral nerves, near knee joints, in the urether or female urethra, in the prostate, urinary bladder and genital organs of both sexes, in the middle ear cavity and tympanic membrane of the ear canal, in and behind of the pancreas, in the neighborhood of the solar plexus, near the retroperitorium and on the olfactory bulb [8, 39, 44–61].

In animals; such as monkeys, beats, elephants, ant-eaters, domestic cattle, slow loris, opossums, tree shrews or platypus, the existence of PCs have been observed [15, 39, 62–68]. Additionally, avian species have a PC like receptor which is known as the Herbst corpuscle [39, 69, 70]. The distribution of PCs within the higher vertebrates' species is quite different from human body. It is very easy to find PC in the mesentery of cat. PCs in cat mesentery have many similarities with the PCs under glabrous skin of human being [71–73]. In average, 141 PCs can be found if only mesentery tissue is considered. However; if pancreas and mesocolon tissues are also taken into consideration, the number of PCs varies between 125 and 627 [74]. Contradictory to

this, there are very few or no PCs in human, dog or rabbit mesentery [57].

PC can be seen with naked eye. This fact enables PC to be one of the most studied and well-known general neural receptor. It is discovered as early as 18th century and identified in 19^{th} century by Filippo Pacini, thus PC is the neural receptor recognized by anatomists.

The function of PC is subject to many speculations even today. Pacini claimed that they were the receptors of magnetic field [41]. It was also suggested that they were a part of lymphatic system or they associated with electric organs in fish and they were thought to be functioning as moisture or osmotic pressure regulators, temperature or pain receptor or sonar detector [1, 75, 76]. Although it is a known fact that PCs are the key elements to sense the mechanical vibrations with relatively higher frequency, its function has still not been discovered in the viscera of cat. Stating that they are connected with a mechanism of vascular regulation, for PCs and blood vessels they are associated with each other in an unknown way [1, 77–86]. It is also claimed that cats are capable of sensing the vibrations of ground using the PCs at mesentery [12]. Regarding to that as a carnivore, the presents of PCs in the ferret is discovered. During an event, they seemed to work together, "synthergizing" the stimulus [87, 88]. Thus, PCs are found in clusters aligned around a common axis [89].

2.1.1 Structure

Because of the similar morphology (Figure 2.2) and the appropriate location to reach easily; the PCs at human finger, mesentery or footpad of the cat are the most studied ones. After the usage of light microscopes to identify the morphology of PCs until 1957, Peace and Quilliam [72] used electron microscope for further investigations with methacylated-embedded material. But Spencer and Schaumburg [89] and Halata [88] used another material called Epon. Methods changed in time such as freeze-fructure studies of Ide [90, 91] or standard fixation, dehydration, osmication or embedding techniques of Bolanowski [24–27, 32]. It is discovered that though each PC

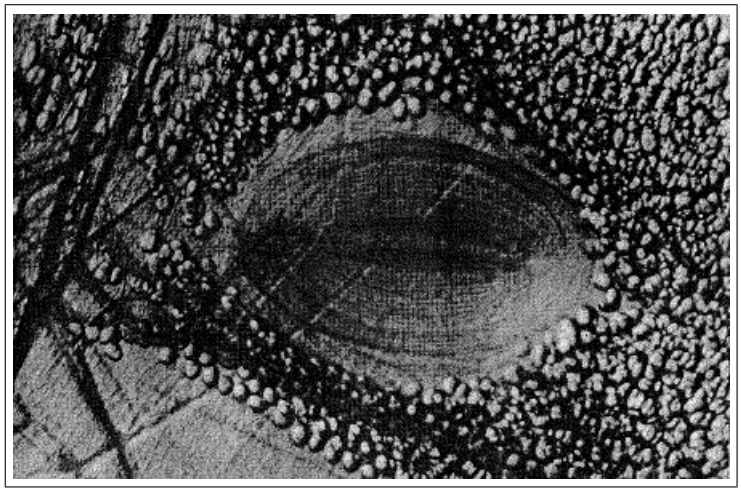

Figure 2.2 A PC with clear morphology view in ovoid shape under 80 x magnifications [41].

resemble each other, they have some differences at some level [1, 89, 92].

Basic structure of PC is a dendrite connected to an axon which is conventionally myelinated. The last segment of it, also called as terminal dendrite, is unmyelined and forms a terminal neurite. The neurite is wrapped tightly with non-neuronal cytoplasmic layers [71, 72, 88, 89]. These layers are the place of PC where it is called the inner core. Inner core is surrounded by narrow intermediate layer called intermediate growth zone which separates the inner core from outer core [72, 93]. Outer core is, similar to inner core, formed by non-neuronal tightly packed cytoplasmic layers with interlamellar spaces filled by water-like fluid and other inclusions. The whole structure is surrounded by a number of closely packed connective tissue which is also called the external capsule [72]. The external capsule is the 99.9 % of PC [94, 95]. A cross-sectional view of PC can be seen clearly in the Figure 2.3 and in Figure 2.4 principal components of the PC structure is represented.

It can be said that PCs are relatively large (Table 2.1) [41]. They have an ovoid shape although there are also exceptional complex shaped PCs [56, 89]. Different sizes of PC can be found within a body. For instance, in the mesentery of a cat, PCs are twice as large as the ones in the footpad [89, 96]. The ones in the articular capsule of a knee joint are even smaller than the one in the footpad. In human beings, PCs tend to

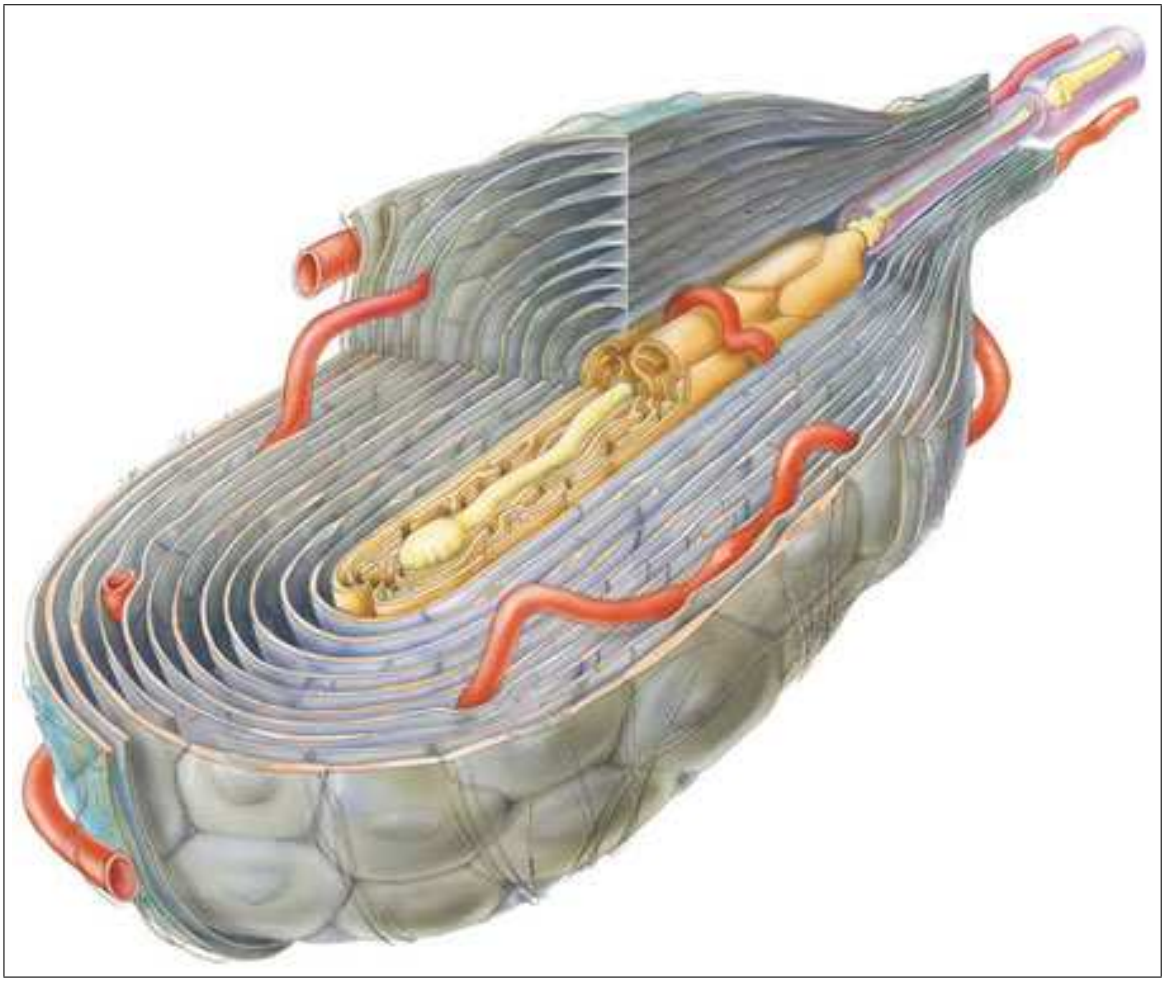

Figure 2.3 A cross-sectional view of PC [Adopted from http://www.scf-online.com/english/26_e/frontpage26_e.htm].

enlarge with age until they are 70. After this age, it is observed that the growth of a PC is regressive. From birth to adulthood, the size of PC changes from 500-700 μm to 3-4 mm. New lamellae are the major growth factors of PC. Lamellae are first noticed at the fourth month of the fetus [1, 7]. New lamellae migrate outwards resulting in the prenatal axon being progressively incorporated into the receptor's accessory structure with age [40]. It is also known that the size of PC is determined with its location. As it is located in the skin, it means that it has more layers in the accessory capsule. So the PC gets larger [88, 97].

In average, a PC is about 10^{-4} cm^3 and weighs between 0.14-0.43 mg. A very big portion of the mass ($\sim 92\%$) is water [95, 98]. It also contains proteins ($\sim 12.6 \times 10^{-2}$

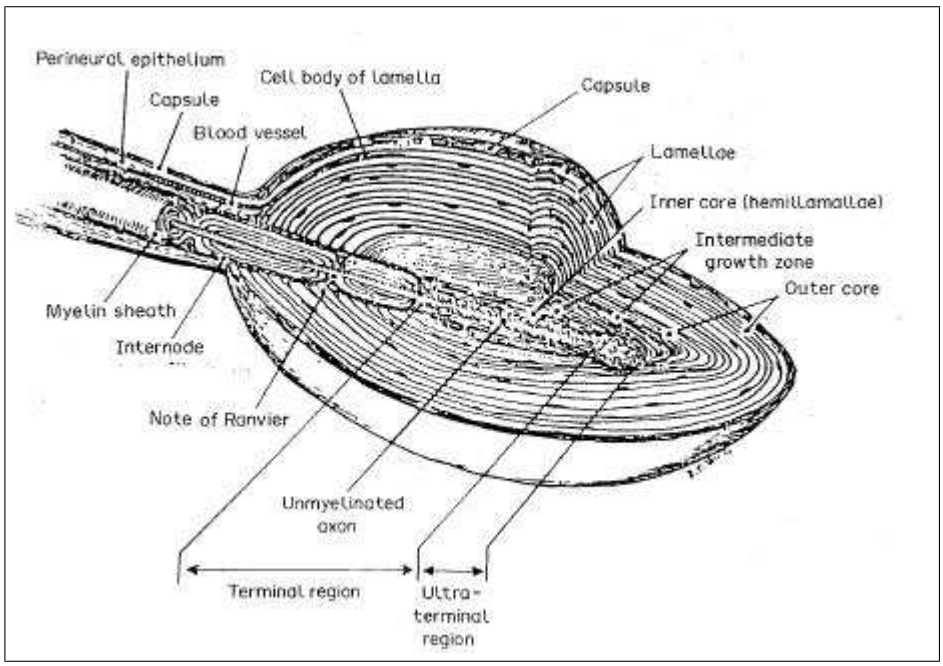

Figure 2.4 Schematic illustration of a PC [41].

mg$\pm 45\times 10^{-5}$) which are both water and salt-soluble proteins and protein-carbohydrate complexes [98]. Proteins play an important role in regulating the metabolic functions in PC. Additionally, actin, which is proved to exist within PC, is a key factor for having structural integrity [99]. Although the amount of K^+ in the fluid of PC is significantly different from blood plasma (6.19±0.72 meq/l in PC; 2.87±0,38 meq/l in blood plasma); the same comment cannot be done for Na^+ content (114.4±10.4 meq/l in PC; 125.6±10.0 meq/l in blood plasma) [100–102]. In spite of the fact that it appears to be from external capsule; it cannot be clearly stated what part of accessory capsule this fluid belongs to [102].

2.1.1.1 Outer core and external capsule. Outer core and external capsule consist of thirty or more successively concentric, flattened, identical cytoplasmic lamellae which surrounds the inner core (Figure 2.5) [72,103,104]. Lamellae contains single layer of tightly fitting cells. Each lamella is separated by a relatively wider fluid space [105]. The fluid space contains a few macrophages, scattered collagen fibrils (especially collagen II), a little ground substance and vascular capillaries [1, 72, 92, 99, 106].

The thickness of this region varies such as it is between 0.03-0.3 mm (with an average of 0.15-0.20 mm.) in the cat mesenteries, except the wider ones in the perincular zone; in the hand of a human it is between 0.09-0.40 mm [72, 92, 107]. The reason for the difference can be explained by the fact that there are more fibrils in the fluid spaces of the lamellae [92].

The radial spacing also varies from 0.15 to 0.815 mm [107]. As the distance from the inner core increases, spacing also increases. To calculate the diameter of outer boundary of n^{th} lamella of the PC, the following formula is given [108, 109]:

$$d_n = d_o D \cdot \gamma^n \tag{2.1}$$

where d_0 is the diameter of inner core and,

$$\gamma = \begin{cases} 1.10 & \text{if } n \leq 10 \\ 1.083 & \text{if } n \geq 11 \end{cases} \tag{2.2}$$

Although, capillary beds allow fluid flow between adjacent interlamellar spaces of a capsule or extracellular spaces between the lamellae of outer core where the blood vessels are; the existence of extensively tight desmosome-like junctions, which play an important role to keep the outer core and external capsule mechanically integrated and structurally stable, is a key factor to hinder the flow [1, 73, 92, 110]. In the first two or three double-celled lamellae of the outer core the relatively dominant tight junctions connect the lamellae over their entire length [110]. The connection of the lamellae with tight junctions may be the reason of the electrically isolation of the inner core fluid from outer core [111–116].

Occasional fibular interconnections between lamellae may be an answer to sepa-

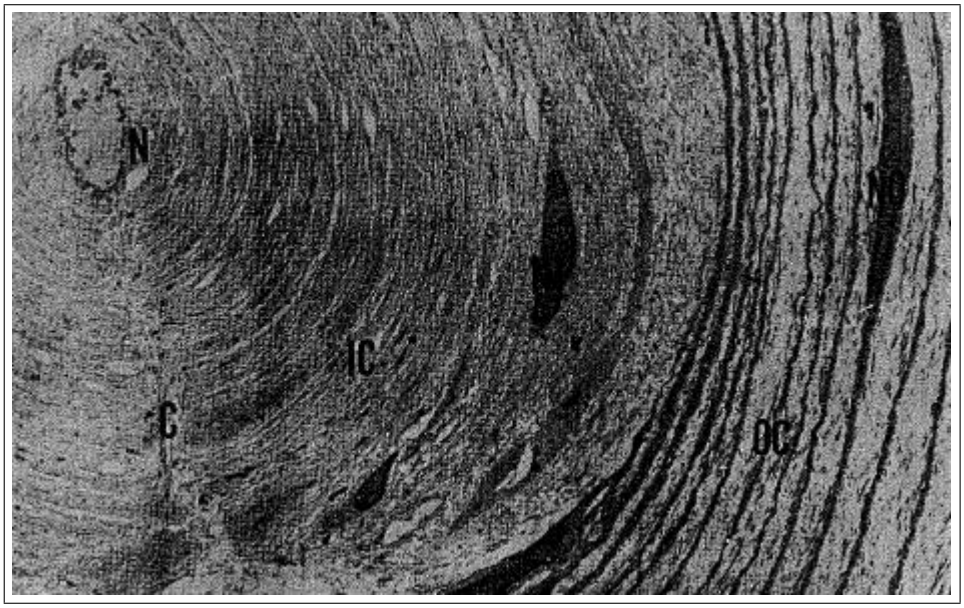

Figure 2.5 Electron micrograph view of a transverse section through the terminal neurite region of a PC, where C is cleft; IC is hemilamellae of inner core; N is elliptical shaped neurite; NI is nucleus of an inner core cell; NO is nucleus of an outer core cell and OC is outer core, and magnified 4000 times [41].

rated membranes, while the stiffness problem is still being questioned. The fluid layers are pressurized so they keep their shape. This is the reason why punctured lamellae collapse [1, 72].

2.1.1.2 Inner core. The inner core is a region in which it contains tightly packed lamellae. The inner core region lies between the neurite and intermediate growth layer. It is 0.8-0.9 mm long and it has 20-40 μm in diameter [103]. Its thickness is about 10 μm thick [117]. The inner core lamellae, contain elongated nuclei and granulated structures [118], are relatively thin (30-40 nm). Additionally, they become thinner the closer to the neurite [119]. They can be either clear or dark, referring to the number of cellular organelles present in each type [93,110]. There also are a sparse accumulation of microtubelis (22nm in diameter); filaments (6-10 nm in diameter), a few mitochondria, Golgi apparatus, endoplasmic reticulum, polyribosomes and vesicles [89, 93, 110] whose flattened nuclei lying on the outer border of the inner core [93] as well as numerous invaginations and vesicles [73] or vesicle-like structures [17, 92, 120] which show up as pits (P-face) and bumps (E-face) in the freeze-factured preparation which are about

10 nm in diameter. The density of the P-face pits is 3,276 per μm^2. The pits are distributed homogeneously. The density of the bumps of the E-face is about 553 per μm^2 which is relatively lower than P-face [62, 73]. Still nothing can be said if the invaginations are involved in pinocytotic or exocytotic activity.

The lamellae cells actually arms from the outer margin into the inner core. The arms appear as concentric layers arranged in bilateral symmetry [72, 92]. The inner core cells and their cytoplasmic which can also be called Schwann cells, have no distinct basal lamina or basement membrane [1, 90, 92, 110, 121]. The calcium binding element called S-100, which exists in glial and ependymal cells of the brain or in Schwann cells, is contained. Thus, Krause [1, 122] proposed that those are also called modified Schwann cells. Outer core or neurite regions do not contain S-100 [99, 123]. It is called modified Schwann cells since non-specific cholinesterase is found on the plasmic membrane, however typical Schwann cells of myelinated axon do not contain this. Moreover, the inner core also contains glial fibrillary associated protein [124]. It is found only in glial cells. Thus, the idea that the inner core cells are probably specialized Schwann cells and are distinctly different to the lamellae cells forming the outer core and external capsule, is further supported [99].

The inner core lamellae are bilaretally symmetrical [72]. They are semi-annular in transverse cross-section; hence the expression "hemilamellae" is used for them [72, 92, 118]. These hemilamellae form two clefts, which contain large fibrils of collagen and small fibrils of elastica as determined from their range in diameters in electron micrographs, which run along the entire dendrite up to the ultraterminal region as seen in Figure 2.5 [102]. The width of the cleft is 0.5-1.0 μm [125]. While within the PCs in mesentery and the fingers of the rhesus monkey there are there are about 60-80 lamellae in each annular section; the PCs in the human hand have roughly one half of it [72, 88]. Unlike the PCs in cat mesentery, in the ones in human hand do not appear to have semi-annular layers [92].

Unlike the outer core, the lamellae of the inner core are closely packed so there is a relatively small amount of fluid between the lamellae. The extracellulalar spaces

Table 2.1
Typical parameter values for mesenteric PCs [17, 71, 72, 92, 125]

Quantity	Value
External dimension of length	1000 μm
External dimension of width	670 μm
Number of lamellae of Outer Capsule	30
Lamellar Thickness of Outer Capsule	0.2 μm
Diameter of Inner Capsule	25 μm
Number of lamellae of Inner Capsule	40-60
Length of Neurite (Unmyelinated Segment)	600 μm
Elliptic Cross Section of Neurite (Unmyelinated Segment) in Minor Axis	2.5 μm
Elliptic Cross Section of Neurite (Unmyelinated Segment) in Major Axis	5.7 μm
Diameter of Myelinated Axon	5.8 μm
First Node Ranvier of Myelinated Axon (into PC)	247 μm
Hemi-node of Myelinated Axon (into PC)	496 μm
Fluid Content in Outer Capsule	2×10^{-4} μl
K^+ in Fluid of Outer Capsule	6.19±0.72 meq/l
Na^+ in Fluid of Outer Capsule	114.4±10.0 meq/l

contain amorphous ground substance, fine filamentous material and collagen-like fibers [73, 90, 106]. There also is a small amount of tubulin [99]. The thin collagen-like fibers are about 15 nm in diameter; however the ones near the clefts are 30 nm [119]. For another difference from the intercellular spaces of the outer core and external capsule, the collagen-like fibers between the lamellae of the inner core run longitudinally [88, 89, 126].

Additionally, the inner core has a number of gap junctions between adjacent cells in each half which is bordered in 0.02 μm^2, densing at the tips against the cleft regions [73]. On the other hand, there are none between cells of opposing sides [110]. The gap junctions may enable to establish isoelectric potential on each side of the cleft only if they act as intercellular channels [110]. Furthermore, between lamellae, desmosome-like junctions can also be found [62]. The tightly bound inner core cells probably regulate the environment surrounding the neurite since the probably receive nutrients

[62,73,90,110,125]. It has been investigated that the tight and desmosome-like junctions probably prevent interlamellae movement of fluids and act as a permeability barrier to ions and molecules along the extracellular regions. It can also be suggested that they are the reason to maintain the structural integrity of the corpuscle. Although the lamellae and the nerve fiber the existance of the desmosome-like structures observed, no synaptic vesicles were found which shows that they are not synaptic structures [73].

2.1.1.3 Intermediate layer. This layer is a transition zone between inner and outer core. This region can be observed in immature PCs as in Figure 2.6. The width of this transition is about 1-1.4 μm [92]. It appears continuous with the endoneurium and includes similar inclusions to endoneurial connective tissue which are [106, 118]:

Collagen fibrils

Microfibrils

Fibroblasts

In this layer, macrophages have also been observed. Thus, it can be considered that the intermediate layers are the endoneurial cells of non-specialized parts of nerve [110].

It can be observed in freeze-fractured preparations that cells do not have basal lamina and possess a low density of intramembrane. The loss of nuclear membrane and condensed chromosomes shows that there is the mitotic activity in this region. This is why the region is also called an intermediate growth zone [110]. The lamellae of the zone are either included by inner core or outer core in time thus in mature PC this region cannot be observed [72]. It is still not discovered what role the zone has in the mechanotransduction process.

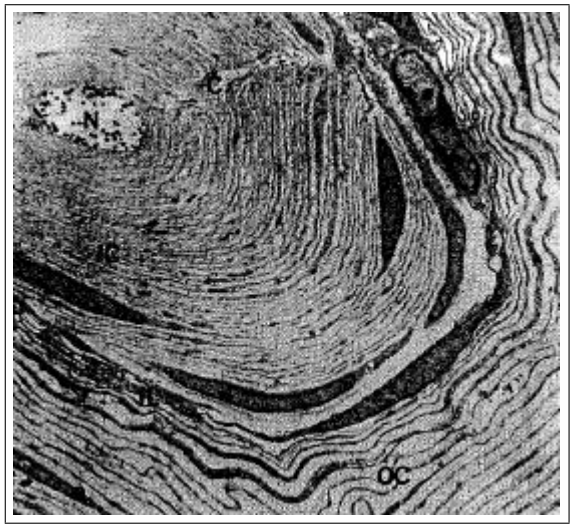

Figure 2.6 Electron micrograph view of a transverse section through the terminal neurite region of a PC, where IC is inner core; OC is outer core; IL is intermediate layer; N is neurite and C is cleft, and magnified 9000 times [41].

2.1.1.4 Neurite. The structural properties of the PC are given detailed above. However, the most important part of this study is the transition part between the PC and the neurite which is located at the core of the PC to understand the structure, and to comment about the results matching different data set. Thus, as much as PC, the neurite should be well understood before the function is covered.

The neurite within the PC can be considered in three distinct regions [91]:

1. an afferent, myelinated preterminal segment located outside the PC.
2. a middle, unmyelinated region called the terminal region within the inner core.
3. a bead-shaped ending called ultraterminus.

In the terminal region, the afferent fiber is generally divided into two or more branches which progress through the inner core. Each of the branch ends with an ultraterminal arrangement [1, 41, 71, 73, 90, 118].

The axon, which has a circular cross-sectional view, innervates the PC [17]. It is myelinated outside of the accessory which has about 3-11 μm diameter [17, 71, 93].

The myelin terminates where the axon enters the accessory capsule at birth, however, at maturity the myelin continues into the PC and there is typically a node of Ranvier about 250 μm into the PC proper [71, 118]. Thus, the first node of Ranvier outside the PC is about 50 μm away from the proximal pole of the capsule [71]. Within the corpuscle the neurite takes a tortuous path making several, right-angle turns. Between the modified Schwann cells and the lamellar cells of the outer core, there is a space filled with many bundles of collagen protofibrils. It is called hemi-node [89] where the myline is lost on neurite within the corpuscle. The node is about 250 μm away from past the node of Ranvier. It is called hemi-node since it resembles half a node of Ranvier. The Schwann cell sheath lasts a few microns away from the hemi-node in distal direction at where point inner core and terminal region begin [89, 118]. In time the number of nodes of Ranvier in the PC may change. It is possible to find two or even three nodes of Ranvier within a PC, however in general there is only one [42].

The terminal region is a straight dendrite, about 600 μm long. It has elliptical cross-sectional view, with one-half the area of the myelinated portion [71]. The ratio of the major to minor axis is not determined for there are different values in different studies (2.35 ± 0.31 [17], 2.26 ± 0.44 [125, 127]). Using different types of microscopes lead this situation. Another interesting point is that many sensory endings have an ellipsoidal shape which is the reason of the proposal of the hypothesis that argues the shape of the neurite may determine some of the neurophysiological properties of the PC [128, 129]. This distinct problem will not be held in this study.

A small amount of PCs in human hand is divided by neuritis into several separate segments in a single PC. A PC with multiple branches of terminal can be seen in Figure 2.7. It is a cross-sectional view of a PC in cat mesentery [90]. This is a very unusual way of innervations. During this study, this type of innervated PCs is taken neither for experiment nor to modeling.

A number of mitochondria are contained as well as bundles of neurofilaments, which have 10 nm diameter, and neurotubules, which is 22 nm in diameter, in the neuroplasma of the terminal region. There also are a sparse tubular reticulum, groups

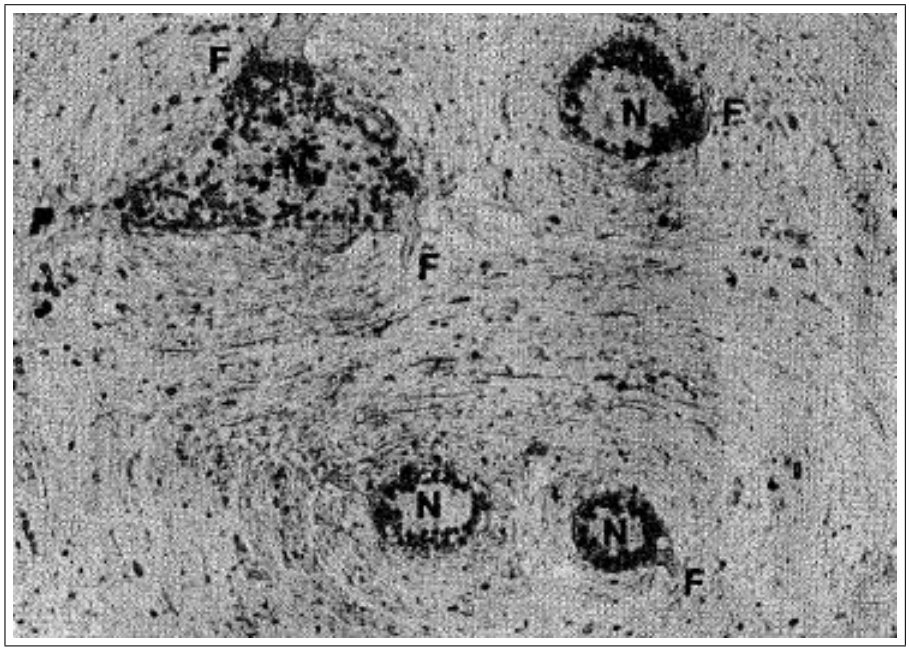

Figure 2.7 Electron micrograph view of a transverse section through the terminal neurite region of a PC with multiple branches of the innervating neurite, which is magnified 6400 times. The separate inner core regions surround the individual neurite processes (N) which have finger-like projection or filopodia (F) projecting into the clefts formed by the gaps separating the inner core hemilamellae [41].

of clear and coated vesicles, lysosomes multivesicular bodies and glycogen granules [17, 89, 118, 120]. The application of polyclonal anti-tubulin factor shows the presence of both alpha and beta subunits of tubulin while intermediate size filament is found by the application of monoclonal anti-neurofilament factor [99]. Additionally, the mitochondria lie parallel to the neurite length [89, 120]. The typical cross-sectional view of a PC can be seen in Figure 2.8 in which the normal inclusions are labeled.

The structure is called filopodia which is the thin processes along the terminal neurite, projecting into the clefts formed by the hemilamellae [66, 89, 92, 93, 118]. The filopodia does not have a regular shape. Its width varies from 0.5 to 1.6 μm [92].

Filopodia is a cytoplasmic extension that resembles neuronal growth cones and axonal spines [90]. The filopodia connected to the 3 to 6 hemilamellae of the inner core, which are located closest to the core, with intercellular gaps. The gaps are bifurcated by filaments and their length is about 8-9 nm, with 3-5 nm diameter [89]. There is an abundance of collagen within the intercellular space of inner core lamellae [92].

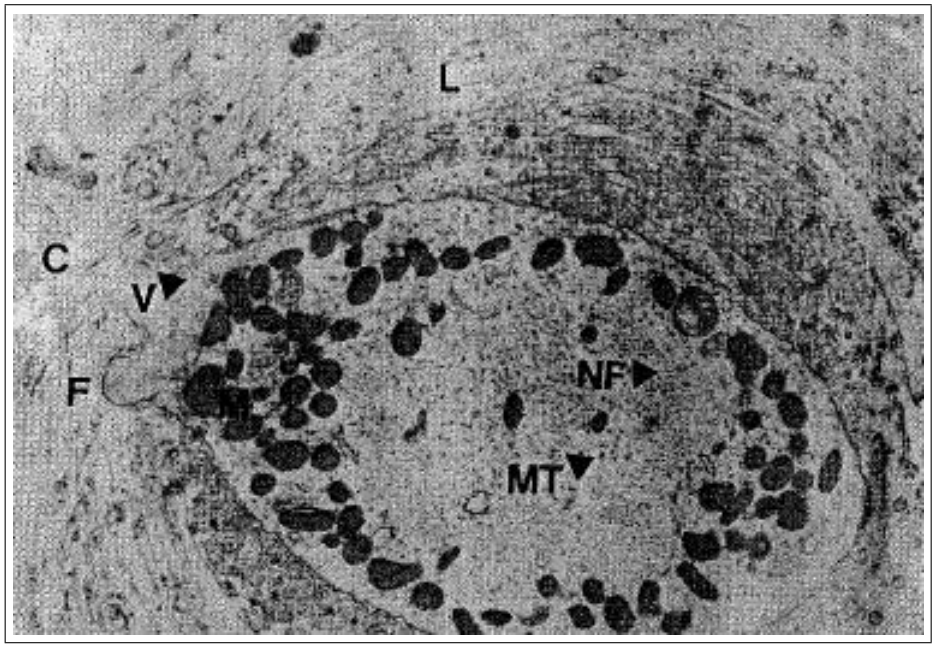

Figure 2.8 Electron micrograph view of a transverse section through the terminal neurite region of a PC magnified 19000 times, with various cellular inclusions within the elliptically shaped neurite. In the figure M is mitochondria; NF is neurofilaments; MT is microtubules and V is vescicles. A filopodia (F) projecting into the clefts (C) is formed by the hemilamellae of the inner core [41].

Filopodia is thought to be ubiquitous to rapidly adapting vibration receptors [99]. The types of filopodia within the PC can be seen in the Figure 2.9 [41]. It was proposed that the filopodia can be categorized into two groups according to their shape and size [99, 130]. One group has a finger-like shape while other group has mushroom-like shape. Though the significance of these differences has not been indicated yet, it is possible that they may cause functional differences in PC. In this study, the possible difference is assumed to be zero.

No mitochondrion has ever been observed within the filopodia however, there are a number of them at the base of filopodia with vesicles, multivesicular bodies and autophagic vacuoles. Additionally, the existence of interconnected microfilamentous with 6 nm diameter, which connect with the axolemma of the filopodia, is observed [66, 130, 131], although it was claimed that there were no neurofilaments [89]. It was also reported that subsurface axolemma is located about 7 nm beneath the surface membrane at the base of each filopodia [89].

The filopodia contain two more types of vesicles [89, 93]:

1. strongly electron-dense, small and resembling, found in synapses.
2. weakly electron-dense and large resembling, found in the inner core.

These vesicles are thought to be released during excitation and believed to be associating with the transduction process. However, both receptor-potential event and the latency between the stimulus and the receptor potential prove that it is not possible, at least in reference to direct mechano-electric conversion. They may have function in nutrition or modulation [66].

It is strongly believed that the receptor potential is originated at the site where is formed by the filopodia and their basal region considering their ultrastructural evidence [66, 72, 89, 92]. This suggestion strengths the belief that there are more than one spot that the receptor potential is generated [27, 32, 95, 132].

The most distal part of the neurite, which is about the last 10-20% of the entire neurite, is the ultraterminal region, where more axonal processes occur (Figure 2.10) [41,89]. In this region the structure of the neurite is not consistent but it generally divides into 2-5 branches that are 50-100 μm long and have a bulbous ending with a diameter of 8-12 μm [71, 89]. The bilateral symmetry of the inner core cannot be observed at this region which leads to the connection of the filopodia with the matrix of basal-lamina like material [89, 133]. It appears as a mace as the structure of the ultraterminal region with the numerous processes that branch from it [120].

2.1.2 Function

When a deformation is applied to the surface of a PC, it produces a non-regenerative, non-propagated receptor potential (RP). If the RP exceeds a threshold

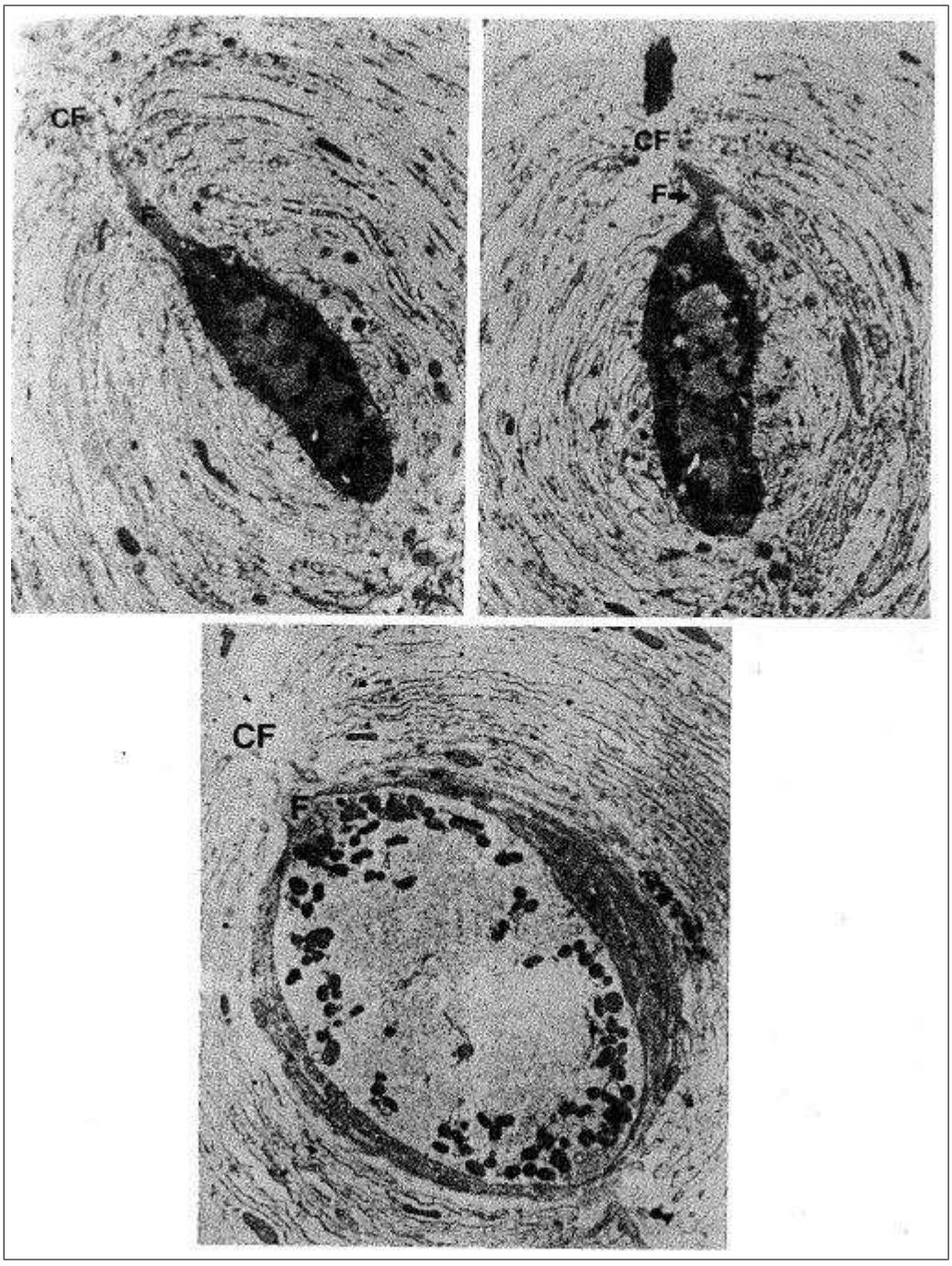

Figure 2.9 Electron micrograph views of a transverse section through the terminal neurite region of a PC, which are magnified 10000 (upper micrographs) and 11400 (lower micrograph) times. It can be seen that a filopodium (F) is projecting from the neurite into the cleft region (CF) [41].

Figure 2.10 Electron micrograph view of a transverse section through the ultraterminal region of a PC where N is neurite; L is lamellae and n is nuclei of lamellae cells [41].

value, it becomes a regenerative and voltage-dependent potential which is called action potential (AP). It is conducted with a velocity between 13-56 $msec^{-1}$, which is a normal velocity considering the axon diameter to be 4-10 μm, to the central location along the afferent axon [134].

PCs are assumed not to be spontaneously active elements. They need mechanical stimulation to generate AP [135]. The accessory capsule and inner core are not required to obtain transduction. However, the accessory capsule acts as a key factor in regulating the ionic environment around the neurite and provides the mechanical filtering of the stimuli applied [26, 27, 94, 136, 137].

The generation of APs occurs when underlying transmembrane voltage change takes place. The voltage change is called generator potential (GP). Thus, to produce an AP in a synaptic mechanoreceptor, GPs, RPs and APs are all produced.

Some techniques have been developed to do experiments on PC [8, 12]. Using the methods, the RPs and APs are obtained from extracellular measurements. The measurements are not exact transmembrane potential measurement however; there is a direct proportion between the measured APs and RPs with the transmembrane potential [27]. Many types of stimulations have been used such as impulse stimulations, ramp-like stimulations or sinusoidal stimulations. Each type of the stimulation is applied to measure and determine different characteristics of the PC. It is mentioned what type of stimulations are used in this study and the reason is also indicated within this text.

2.1.2.1 Receptor and action potentials. After a number of experiments, Gray and Sato [111] claimed that they separated APs from RPs. With the usage of three phased recording apparatus, the response was recorded. In the first phase with the change of stimulus, the change response in response is observed. Thus, the first phase was RPs. In the second and third phase recordings, it was observed that the responses had all-or-none behavior which means the second and third phases were APs. The second one was initiated within the corpuscle while the third one was recording was taken from myelinated afferent fiber emerging from the corpuscle. It was claimed that the decrease of electrochemical gradient of ions cause the APs. Thus, the action is originated as the membrane is stretched which caused the opening of unidentified ion pathway. However, the theory was disproved because of the short latencies between stimulus onset and receptor potential initiation

Loewenstein and Altimirano-Orrego [138, 139] claimed the distinctiveness of the RP and AP with additional proofs. It was found that a refractory period occurs after a RP which affects the subsequent RP inversely proportional. The same behavior is obtained after an AP affecting the next AP although it has no effect if the next generation is a RP. It was also stated that electrical stimulation caused APs but no RPs were observed which supports proposed the idea that RPs and APs are independent and maybe even separated from each other. Moreover, it was also observed that there is a constant latency between stimulation and RPs while intensity-dependent latency

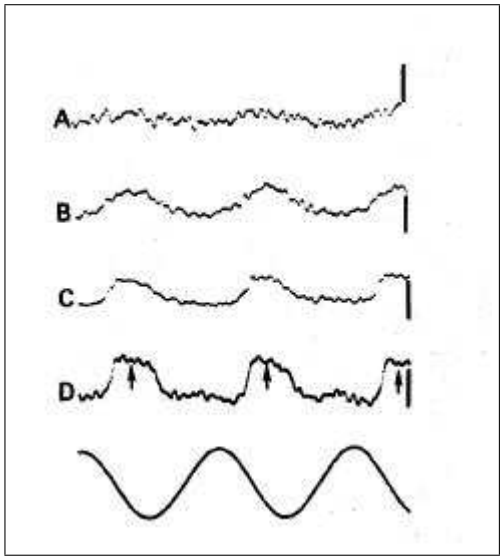

Figure 2.11 Signal averaged RPs in response to a 150 Hz sinusoidal stimulus whose amplitude is increased from A to D. The APs are eliminated [41].

between stimulation and APs.

Although the both studies were successful in determining the separate sites where APs and RPs initiated, they could not spot them. Loewenstein and Rathkamp [94, 95] succeeded to spot the AP initiation site by using fine steel hook. It was also stated that AP set up site is not on the terminal neurite otherwise no AP propagation is observed [117]. There are generators at the unmyelinated ending which are independent from each other. The generators can only be stimulated be mechanical stimulation where is not associating the AP propagation as stated [140]. The originating site of RPs is claimed to be unmyelinated portion of the dendrite [113, 114, 138, 139].

In other studies it was also claimed that surface membrane is responsible for the generation of APs [137] while another one claimed terminal neurite [141] or the other one stated the first node of Ranvier was the site of AP origination [117]. There are many studies can be found to further deepen to find an answer to the question where the APs are generated [115–117, 135, 137–139, 141–143]. However there is no common belief that whether in normal physiological functioning the AP is generated on the terminal neurite or at the first node of Ranvier.

It has been found that when long-lasting mechanical stimuli are applied both hyperpolarization and depolarization RPs may occur as different reactions to the two phases of stimulation [144]. The comment agrees with the results of Bolanowski and Zwislocki [27] although the amplitude of the stimulus plays a major role in producing a given response. In the literature "inhibiting receptor response" and "excitatory receptor potential" terms were used [144]. Today instead of those terms "on" and "off" is used [145]. "On" response is obtained using smaller amplitude than the ones used to generate "off" response. Additionally, some PCs had equal "on" and "off" responses. The recoil deformation of the capsule is the reason for "off" response, which can be also called modified "on" response.

In sinusoidal stimulation, the produced RP is more complicated than that obtained using either pulse like or triangular stimuli. The measured RP values are shown in the Figure 2.11 after vibratory stimulation [27]. Their findings show that the amplitudes of RP and the applied sinusoidal stimulation there is an interesting bound which is at 250 Hz a plateau is obtained. To eliminate it a band-pass filter is applied [26].

2.2 Previous PC Models

There are so many studies on PC aiming to find the unknowns about it. On the contrary, very few of them used model to explain the behavior. Especially, there are three studies in which models, that can be included as detailed quantitative continuum, are proposed [2–4]. The capsules are assumed to be in cylindric geometry with concentric, elastic, cylindrical membrane shells for lamellae and viscous and incompressible shell for interlamellae fluid in these studies.

In the model of Loewenstein and Skalak [2] the core region is assumed to be rigid. The connections between lamellae are set up to be weak. The inertia is ignored and only one pressure mode is used to simplify the model. Instead of solving the equations, an electrical equivalent to the model is created and the model is solved on this analog. The model was successful considering the results of Hubbard [109]. The displacement

curves of static and dynamic stimulations are similar in these studies however there is a distinct quantitative difference. It may be caused by Hubbard's unnatural displacement stimulations [109]. On the other hand the most important difference of the results of these two studies is not the quantitative distinction. It is the place of peak point of the displacement. In Loewenstein and Skalak's model's results [2] it is close to the core however, in Hubbard's results [109] it is observed to be happening earlier. It may be because of the rigid core. While the transient components of the displacement of these two studies are similar, the recovery time for the transient effect in static displacement for both studies does not argue. An interesting point in their findings is that after compression, the amplitude of the negative undershoot is claimed to be larger. It was concluded for the fact that the second receptor spike is usually larger than the first one.

In 1990 a model for capsule is proposed by Holmes and Bell [3]. The ideas of the model were based on the expressions stated by Loewenstein and Skalak in 1966 [2]. It was the capsule which was thought to be forming by concentric elastic membranes separated by viscous and incompressible fluid. Thus, a two-dimensional cross-sectional capsule model which can be thought of as a limiting (slender body) approximation to the full PC capsule is proposed. The orientation of the fibers as well as the local nature of the excitation of the dendrite led to this model. The model is assumed to be homogeneous by assuming the layer thickness is much smaller than the capsule radius. The simplest boundary conditions were applied for stimulation. The physiologically atypical boundary conditions made the results very hard to match the previous results [2, 109].

In the subsequent study, published in 1992, [4] the model was considered to be divided into two general components, one for the mechanics of the capsule and one for the electrophysiology of the nerve fiber. The mechanical capsule and electrophysiological dendrite are coupled through the hoop strain. As the previous model concentric elastic membranes characterizing the lamellae are separated by fluid layers as shown in the Figure 2.5. There is no change in the mechanical model part however the change is, what is coupled with it. It is stated that the terminal neurite is as long as 800 μm while

its diameter as about 4 μm. Thus, a passive cylindrical cable is modeled with active filopodia. A modified Hodgkin-Huxley (HH) cable model is used in which the active membrane currents were associated with each filopodium head. From the heads, ionic current is obtained which includes transducer current. The transducer current can be thought to be activation variable dependent on strain in the receptor membrane which was derived from Eyring's absolute reaction rate theory [146, 147]. This model had more convenient results comparing the previous one. Physiologically logical boundary conditions may be associating with it.

2.3 Finite Element Method (FEM)

The finite element method is a numerical method that is used to calculate the accurate solution of complex engineering problems. The solution approach is based on both eliminating the differential equation completely and rendering the partial differential equation into an equivalent ordinary differential equation, which is then solved using standard techniques such as finite differences.

In partial differential equations, the primary challenge is to create an equation that approximates the equation to be studied, but is numerically stable, meaning that errors in the input data and intermediate calculations do not accumulate and cause the resulting output to be meaningless. There are some certain ways of doing this, all with advantages and disadvantages. The finite element method is a good choice to solve partial differential equations over complex domains, when the domain changes, or when the desired precision varies over the entire domain.

The finite element method is a method in which the solution region is considered as built up of many small, interconnected sub-regions which are called finite elements. A convenient approximate solution is assumed. Then, the conditions of overall equilibrium of the structure for each piece or element are derived. The satisfaction of these conditions results an approximate solution for the displacements and stresses.

Although the method can be said to be first developed in 1956 [148], actually its concept has been used centuries ago, only it was not named as finite element method. For instance, ages ago the mathematicians found the circumference of a circle by approximating it by the perimeter of a polygon as shown in Figure 2.12. In present day notation, "finite element" denotes each side of the polygon. A lower bound $S^{(l)}$ or an upper bound $S^{(u)}$ for the true circumference S can be obtained considering the approximating polygon inscribed or circumscribed. Moreover, the circumstance approaches to the true value as the number of sides of the polygon is increased. This is the characteristics of the finite element application. In 1943, a similar approach to the finite element method was suggested which was involving the use of piecewise continuous functions defined over triangular regions [149].

The development of finite element method with its real term was for the analysis of aircraft structural problems [148]. Theoretically, the whole system was considered to built up simple finite elements (pin-jointed bar and triangular plate within plane loads), and the analysis of aircraft structure was done using finite elements. this study can be considered as the one of the early and key contributions in the development of the finite element method [148]. The development of the computer technology made the method give more precise results for the high capacity of calculation which provides smaller finite elements. Although, It was presented that the finite element method is suitable for the solution of stress analysis problems the method can also be used for every type of physical problems [150, 151]. It is possible to derive finite element equations using a weighted residual method such as Galerkin method or the least squares approach which shows the broad interpretation of the finite element method. As a result, the method started to be used by mathematicians in the solution of linear and nonlinear differential equations. In time, the method has been so popular that many projects, articles or conferences conducted many results using or involving finite element method.

The finite element technique has been so well established recently. Today it can be considered to be one of the best method to solve a wide variety of practical problems efficiently. Especially for complicated boundary problems, the method can be used. In fact, both ordinary and partial differential equations the method is valid to be used.

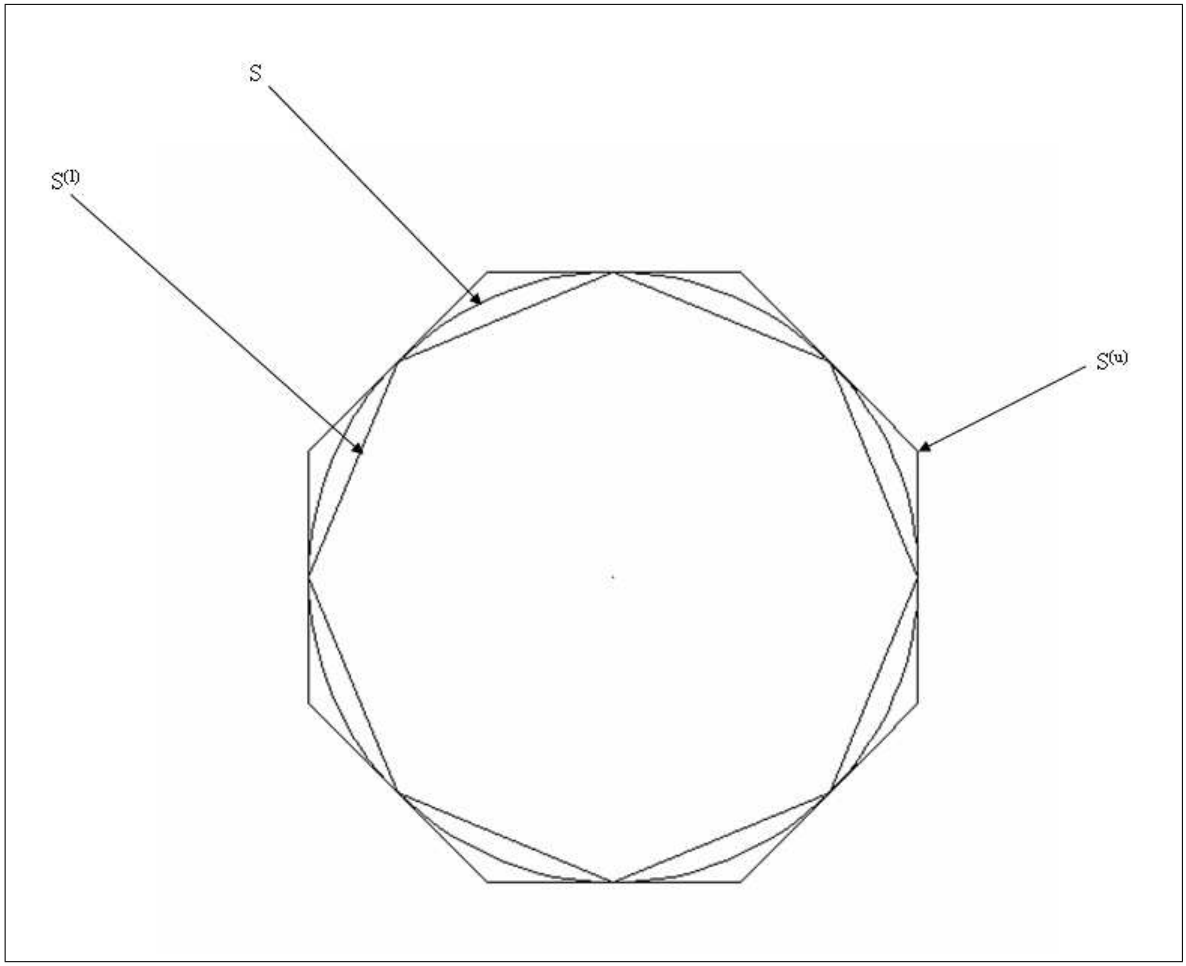

Figure 2.12 Polygons are used to calculate the circumference of the circles for the fact that circles are also polygons with infinite number of sides.

Because of the general applicability of it, various types of engineering problems can be solved using the finite element method.

As mentioned, although the finite element method was first performed for aircraft analysis, it can be applied to various boundary value problems in engineering. A problem is called boundary value problem when the solution is attempted to find in the domain of a body subject within the satisfaction limits of prescribed boundary conditions on the dependent variables or their derivatives. As stated in the Appendix - A, there are specific applications of the finite element method in the three major categories of boundary value problems:

1. equilibrium or steady-state or time-independent problems.
2. eigenvalue problems.
3. propagation or transient problems.

In an equilibrium problem, the steady-state displacement or stress distribution is tried to find in solid mechanics problem; temperature or heat flux distribution is sought in a heat transfer problem; and pressure or velocity distribution is needed in a fluid mechanics problem. One part of the current study is equilibrium problem.

The eigenvalue value problems can be considered to be an extension of equilibrium problems. The only difference is that, critical values for certain parameters are needed to be determined in eigenvalue problems in which time does not appear explicitly again. In eigenvalue problems, the natural frequencies or buckling loads should be found primarily in a solid mechanics or structures problem; stability of laminar flows is sought in a fluid mechanics problem; and resonance characteristics is tried to be found in an electrical circuit problem.

Unlike the problems listed above the propagation or transient problems are time-dependent. The response of a body under time-varying force is wondered in solid mechanics; and the response under sudden heating or cooling is sought in the field of heat transfer.

Finite element method is generally used to simulate of physical systems. Since, for this purpose a model is used, the methodology is named model-based simulation.

The model-based simulation process is illustrated in Figure 2.13. The configuration of the system is called physical FEM, because in the centerpiece the physical system exists. Both idealization and discretization processes enable to produce the discrete model. The equation solver, which is customized to FEM, gives the discrete solutions.

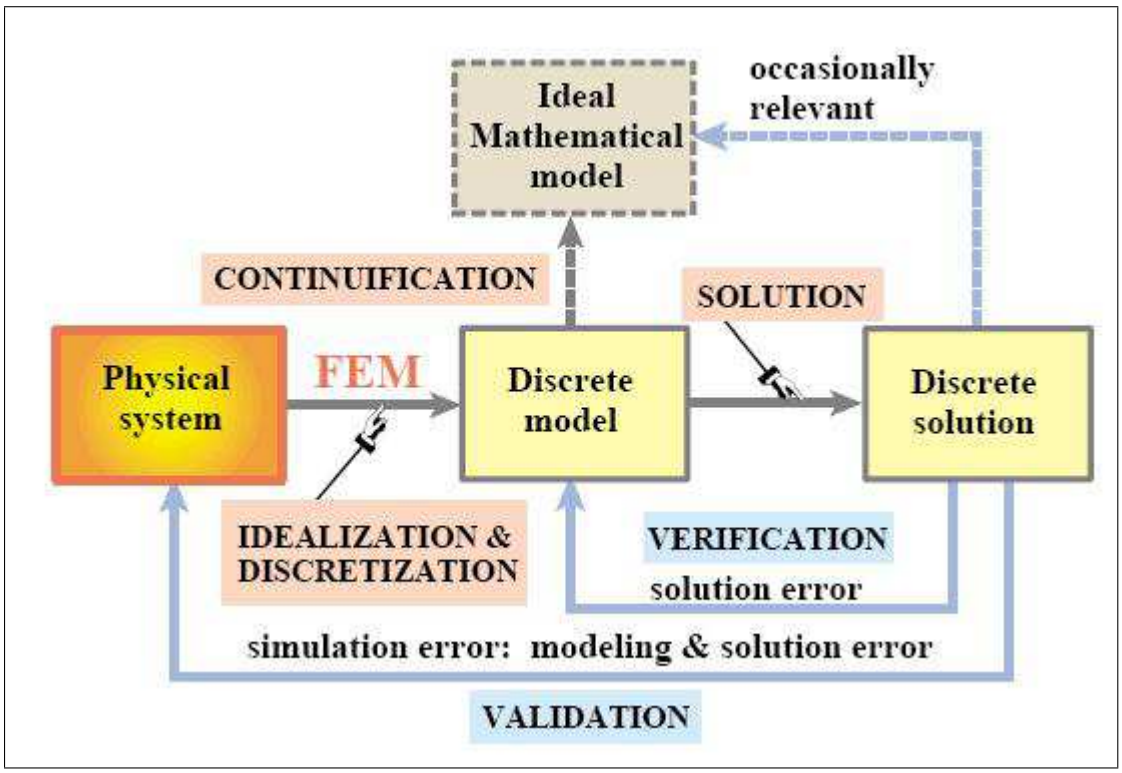

Figure 2.13 Physical FEM process in block diagram [Adopted from http:// www.colorado.edu/engineering/CAS/courses.d/IFEM.d/ IFEM. Ch01.d/IFEM.Ch01.pdf].

A matter is called continuum if it involves a gradual quantitative transition without abrupt changes or discontinuities. In the finite element method, the body of matter can be divided to the sub-regions or finite elements as long as the matter is continuum. Each element is interconnected to the adjacent one at specified joints. These joints are called nodes or nodal points and lie on the element boundaries. Since the actual variation of the field variable inside the continuum is not known, a simple function, defined in terms of the values of the field variables at the nodes, is assumed to be approximating the variation of the field variable inside a finite element. Stating the field equations for the whole continuum, the new unknowns are revealed to be the nodal values of the field variable which can be known by solving the field equations. Then, as a next step, the field variable throughout the assemblage of elements is defined by the approximating functions [152].

The solution of a continuum body problem which is carried out by the finite element method always follows a step-by-step process order. As an example, the step-

by-step solution procedure of a static structural problem can be stated as follows:

1. Discretization of the structure: Dividing the structure into subdivisions or elements is the prior step of the finite element method. Thus, the whole structure is obtained to be modeled with suitable finite elements to simulate. The number, type, size, and arrangement of the elements are to be decided accordingly.

2. Selection of a proper interpolation or displacement model: Some suitable solution within an element is assumed to approximate the unknown solution, which must be both simple from a computational standpoint and satisfying for defined convergence requirements, because the displacement solution of a complex structure under any specified load conditions cannot be predicted exactly. Polynomial form is generally used for the solution or the interpolation model.

3. Derivation of element stiffness matrices and load vectors: From the assumed displacement model, the element e from the stiffness matrix $[K^{(e)}]$ and the load vector $\overrightarrow{P}^{(e)}$ is to be derived by using either equilibrium conditions or a suitable variation principle.

4. Assemblage of element equations to obtain the overall equilibrium equations: The individual element stiffness matrices and load vectors are to be assembled in a suitable manner, since the structure is composed of many finite elements. Considering that $[\mathbf{K}]$ is the assembled stiffness matrix, $\vec{\mathbf{\Phi}}$ is the vector of nodal displacements and $\vec{\mathbf{P}}$ is the vector of nodal forces for the whole structure; the overall equilibrium equations can be formulated as follows:

$$[\mathbf{K}]\vec{\mathbf{\Phi}} = \vec{\mathbf{P}} \tag{2.3}$$

5. Solution for the unknown nodal displacements: Boundary conditions are needed to be taken into the account, so the overall equilibrium equations are modified and the equilibrium equations becomes as follows:

$$[K]\vec{\Phi} = \vec{P} \tag{2.4}$$

6. Computation of element strains and stresses: Stress and strain values can be found by solving the necessary equations of solid or structural mechanics since the nodal displacements, $\vec{\Phi}$, are known.

The six-step solution stated above can be extended to the other fields after modification of terminology if needed.

3. METHODS

Structurally non-linear PC has ovoid shape. It is not possible to address fully such problem with an analytical mathematical model. In order to represent experimental findings a solid three-dimensional model is a good choice which would include the possible effects of PC geometry. Finite element method is a very powerful method for such purpose.

In order to understand and address the modeling process, this question should be answered first: What does the model mimic?

3.1 Previous Experimental Assessment

The experiments were done in Syracuse University. For the experiments the PCs in the cat mesentery were used. The experiments had been approved by both Use Committee of Syracuse University and Institutional Animal Care. The procedure of isolating PCs for the experiment was the same as the stated procedure in the previous study [26, 27]. A CCD camera (model TI-50ES; NEC USA, Inc., Melville, NY), which is capable of recording in high magnification, was used to observe the PCs. The camera was placed perpendicular to the stimulus probe, leading a clearer view including inner core and outer core lamellae and external capsule. It was easy to separate the lamellae from fluid space. The lamellae were dense so it appeared darker than bright fluid spaces. The experiments were recorded to a VHS cassette [153]. The model is aiming to mimic this experiment.

There are two types of data set in total besides the model data set. One was obtained from VHS cassette, observing the PC behavior under stimulation. The other one, which is called the physiological data set, was obtained a previous study. It was obtained from nerve recordings, measuring the potential changes due to the stimulation

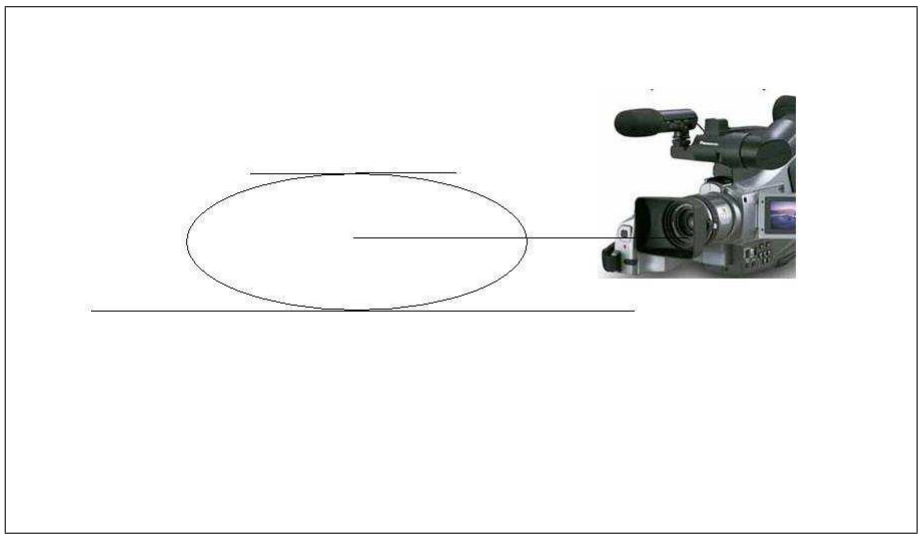

Figure 3.1 The camera is placed perpendicular to the stimulus direction unlike previous studies [109].

(Figure 3.1 and Figure 3.2).

3.2 Model

Although it is essential to construct a finite element model, it must be proven that the model really works and simulates the actual experiment. It is because, the PC itself has a nonlinear structure itself so as its material properties. Considering all nonlinearities, it would be doubtful to accept all the results after simulation without questioning the reliability of solution.

To overcome this problem, a test model is also needed. With suitable material properties implemented, such test model may be used to check for reliability.

In the present study finite element simulations were performed with the use of the ANSYS 10.0 program. ANSYS is a powerful program especially in structural nonlinear analyses. The program allows user to use both graphical user interface (GUI) and BATCH mode. Presently, the analyses were done mostly using GUI and then checking the command line.

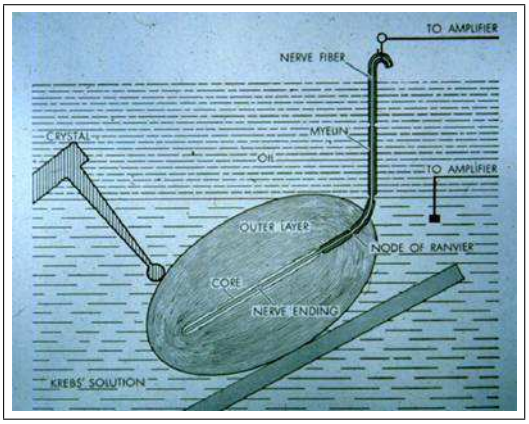

Figure 3.2 Physiological data is collected from the nerve after the mechanical stimulation of the PC [Adopted from http://www.psych.umn.edu/courses/fall05/burkhardtd/psy3031/images/pacinian.jpg].

SolidWorks 2007 was also used to construct the PC solid model.

3.2.1 Test Model

Before dealing with the actual modeling process, the test modeling was held. Because of the purpose of the test model, its geometry is not important.

In order to understand the effect of the parameters input to the program, isolating all other effects that may occur because of various unpredictable reasons, it is convenient to leave all possible parameters out of consideration. Thus, the simplest shape with the least number of elements was needed as the test model.

Firstly, it was thought that only one cubic element should be constructed however, in that case, filtering effect could not be measured. Thus, one element with eight nodes, four of which were constrained fully while others were forced to move in one direction with the given displacement, was not enough to show the filtering effect. All nodes would have had value to move, so there would leave no independent nodes to observe such an effect.

Therefore, a cubic structure was considered using 8-elements (Figure 3.3). This

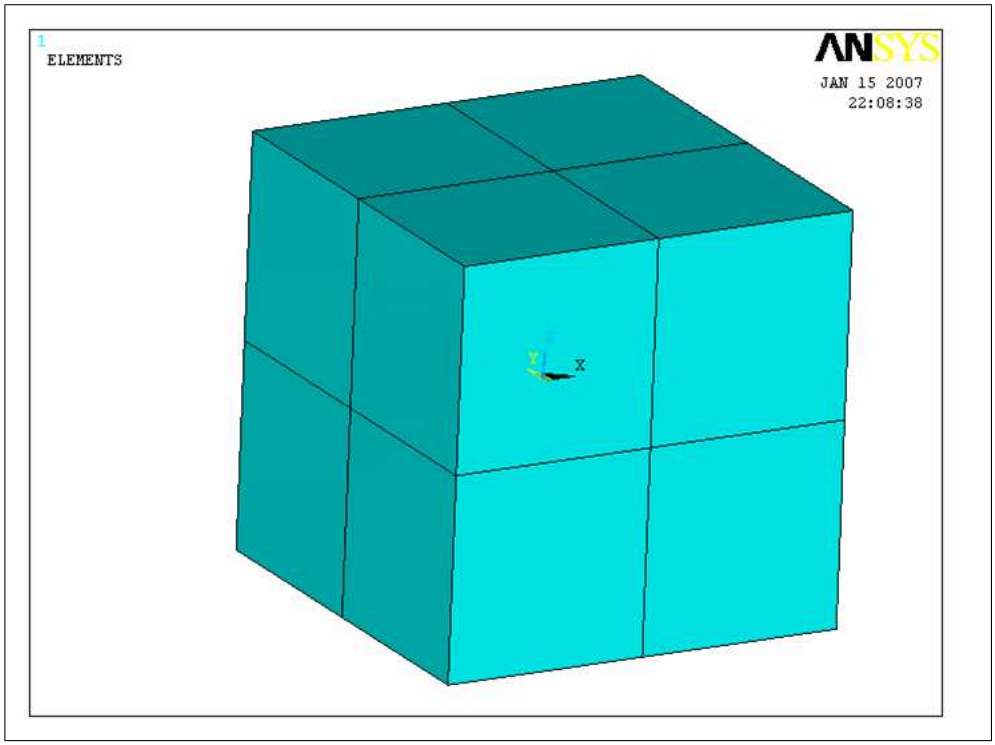

Figure 3.3 The test model.

allows measurement of the effect from the nodes in the middle layer of the model.

The element type was chosen to be SOLID186. Note that the same element was used after for the actual PC model: This allows showing if the element is capable of representing all the needed properties.

On the other hand, based on an assumption, the material properties were set to be different from the actual model. The test model is to test if a material can show filtering behavior under stimulations at different frequencies and, as a result, to determine if the same procedure can be applicable for the actual model. Thus, the mechanical properties were selected in order to ensure that the test model responses as expected. At this point, to make the calculations easier, the simplest viscoelasticity model i.e., Maxwell model was chosen.

3.2.1.1 The Maxwell model. Maxwell model is a viscoelasticity model named after James Clerk Maxwell. It is also known as a Maxwell solid. Maxwell model is

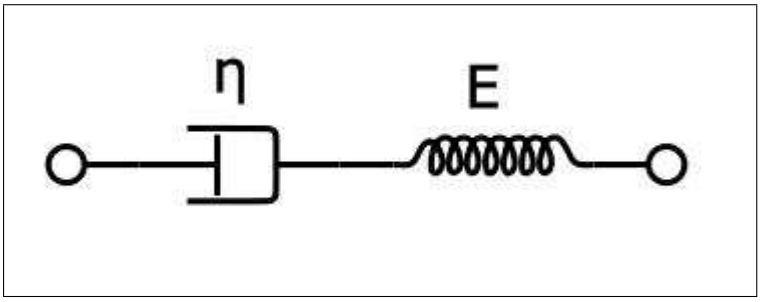

Figure 3.4 The Maxwell model [Adopted from http://en.wikipedia.org/wiki /Maxwell_material].

simply a purely viscous damper and a purely elastic spring connected in series (Figure 3.4).

Considering D denotes damper and S is for spring, the total stress, σ_{Total} and the total strain, ε_{Total} under an applied axial stress can be defined for Maxwell model as follows:

$$\sigma_{Total} = \sigma_D = \sigma_S \tag{3.1}$$

$$\varepsilon_{Total} = \varepsilon_D + \varepsilon_S \tag{3.2}$$

If the strain equation is further elaborated:

$$\frac{\partial \varepsilon_{Total}}{\partial t} = \frac{\partial \varepsilon_D}{\partial t} + \frac{\partial \varepsilon_S}{\partial t} = \frac{\sigma}{\eta} + \frac{1}{E}\frac{\partial \sigma}{\partial t} \tag{3.3}$$

where E is the Young's modulus and η is the material viscosity coefficient. The damper is described by Newtonian fluid while the spring is described by Hooke's law.

The model is applicable for small deformation cases. For the large deformations it should be extended to include geometrical non-linearities.

The viscoelastic Maxwell model is known to act as a high-pass filter under dynamic stimulation. Thus, if the model constructed acts like a high-pass filter as well as predicted, it means that the procedure can be applicable.

Regarding the material properties,

$$G = \frac{E}{2(1+\upsilon)} \tag{3.4}$$

where G indicates shear modulus and E is Young's modulus. Using the relation indicated in the Eq. 3.4, the Prony series in general form can be expressed as follows:

$$G(t) = G_0\Big[1 - \sum_{i=1}^{N} \alpha_i \Big(1 - e^{\frac{-t}{\tau_i}}\Big)\Big] \tag{3.5}$$

where G(t) denotes the relaxation modulus. In the current problem, for Maxwell model, N is equal to 1. In this study, for both test and actual models, viscoelasticity was provided with Prony coefficients. For both models, temperature changes were assumed to be zero, thus the viscoelasticity was independent from temperature. Besides defining the instantaneous response G_0 it is needed to define how much the material will relax, given by α, and the characteristic relaxation time τ.

The transfer function of the model after Laplace Transformation is as follows:

$$\frac{\sigma(s)}{\varepsilon(s)} = \frac{Rs}{s + \frac{R}{\eta}} = \frac{\eta s}{\frac{\eta}{R}s + 1} \tag{3.6}$$

From Eq. 3.6, Eq. 3.7 can be derived in time domain:

$$g(t) = e^{-\frac{R}{\eta}t} \tag{3.7}$$

The equation for the Prony series can be also written as:

$$\sigma_t = \sigma_0 + \int_0^t \dot{g}(\tau)\sigma_0 d\tau \tag{3.8}$$

If the integral is taken within the given interval; then,

$$\sigma(t) = \sigma_0 + \sigma_0(g(t) - g(0)) \tag{3.9}$$

If the function g(t) is expanded:

$$g(0) = 1 \tag{3.10}$$

$$g(t) = 1 - g_i\left(1 - e^{\frac{-t}{\tau_i}}\right) \tag{3.11}$$

Thus Eq. 3.9 becomes:

$$\sigma(t) = \sigma_0\Big[1 - g_i\Big(1 - e^{\frac{-t}{\tau_i}}\Big)\Big] \tag{3.12}$$

If Eq. 3.7 and Eq. 3.11 are considered together the following equations are obtained:

$$g_i = 1 \tag{3.13}$$

$$\tau_i = \frac{\eta}{R} \tag{3.14}$$

The cut-off frequency for the high-pass filter needed to be determined randomly. It is assumed to be 100 Hz. Thus, the following equation can be written:

$$f_{cut-off} = \frac{1}{2\pi\frac{\eta}{R}} = 100Hz \tag{3.15}$$

From Eq. 3.15:

$$\frac{R}{\eta} = 200\pi \tag{3.16}$$

Considering Eq. 3.14 and Eq. 3.16 together, the time constant can be found to be:

$$\tau_i = 0.00159 \tag{3.17}$$

Thus, the needed coefficients were determined for the test model.

3.2.2 Actual PC Model

The developed actual model featured all essential material properties as well as the three dimensional shape of PC. Nevertheless, certain assumptions were made in construction of the model:

1. the PC was assumed to be isotropic.
2. structurally, the PC was considered to be homogeneous. Thus, the lamellae of the PC were not modeled.
3. the environment is considered to be frictionless.

The ovoid shape of PC yields an elliptical shape of the model in the frontal view and a circular shape in the side view. The shape is symmetrical. During the experiment, the PC was standing on a rigid plate as it was being stimulated by a stimulator of a circular contacting surface. The major axis of the PC model was set to be parallel to the rigid surface (Figure 3.5 and Figure 3.6).

According to Figure 3.5 and Figure 3.6, the system is not symmetric with respect to the X-Axis. However, if the structure is thought to be fully symmetrical with respect to the Y- and Z- axes, it would not be wrong. Thus, modeling one quarter of the whole system is considered as sufficient to obtain the results for the whole system.

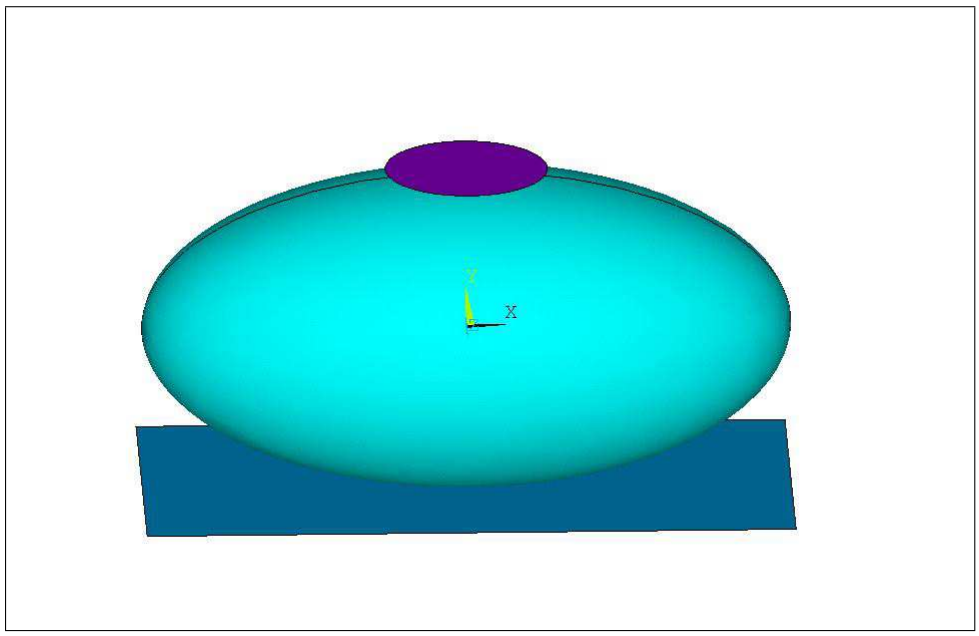

Figure 3.5 The illustration of the experiment in front view.

In order to address the complex shape of the PC, the solid modeling of PC was performed using SolidWorks. One quarter of the PC was modeled with SolidWorks (Figure 3.7). Then, the model was exported as a parasolid model which is a very powerful file format to save all the three-dimensional model data (e.g., coordinates of keypoints) accurately. Note that it is possible to have errors in addressing the model data while the file is exported and imported. To minimize or dismiss the error, an extra effort needed to be performed. It was crucial to have no error in the data of the model; otherwise the system would not work due to unbalancing in frictionless environment.

To make the calculations easier the major axis of the PC model was assumed to be 1 mm, and minor axis is assumed to be 0.5 mm. The major dimension of the PC was chosen to be close to average values as shown in Table 2.1.

After importing the data into ANSYS; a quarter or a rigid plate was put below the PC, considering that it would stand on a rigid plate. The whole plate was thought to be covering all PC so quarter of it was dimensioned as 0.5 mm and 0.25 mm.

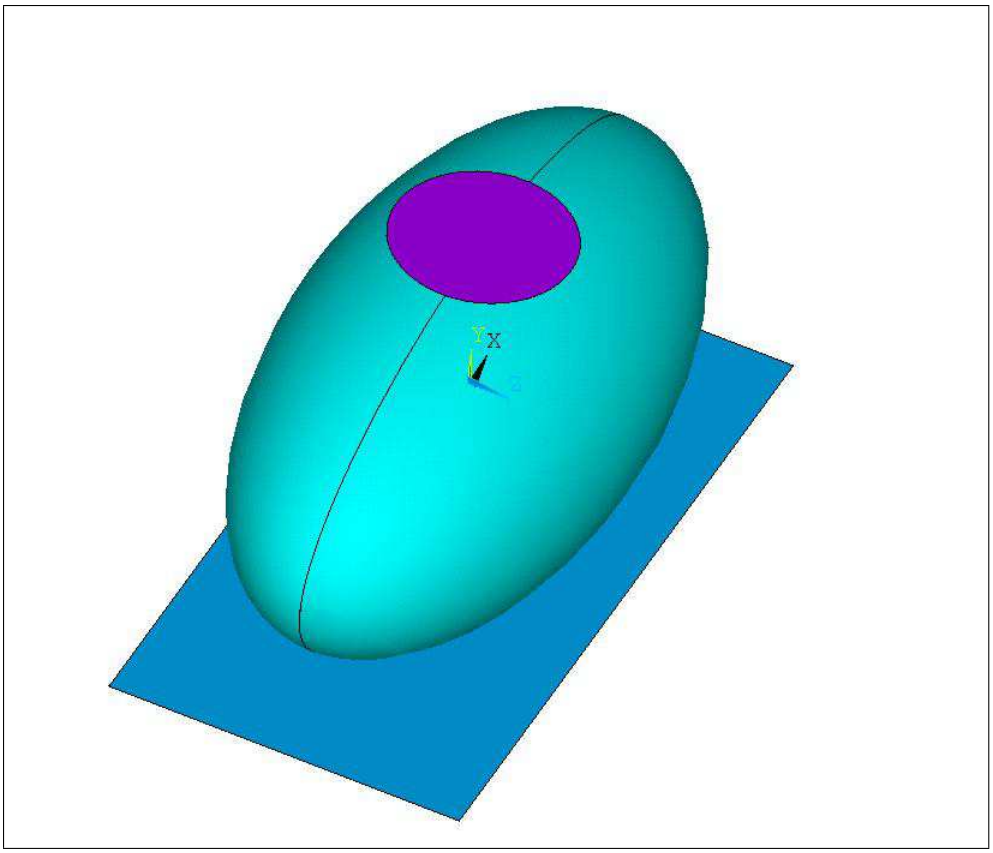

Figure 3.6 The illustration of the experiment in upper right corner view.

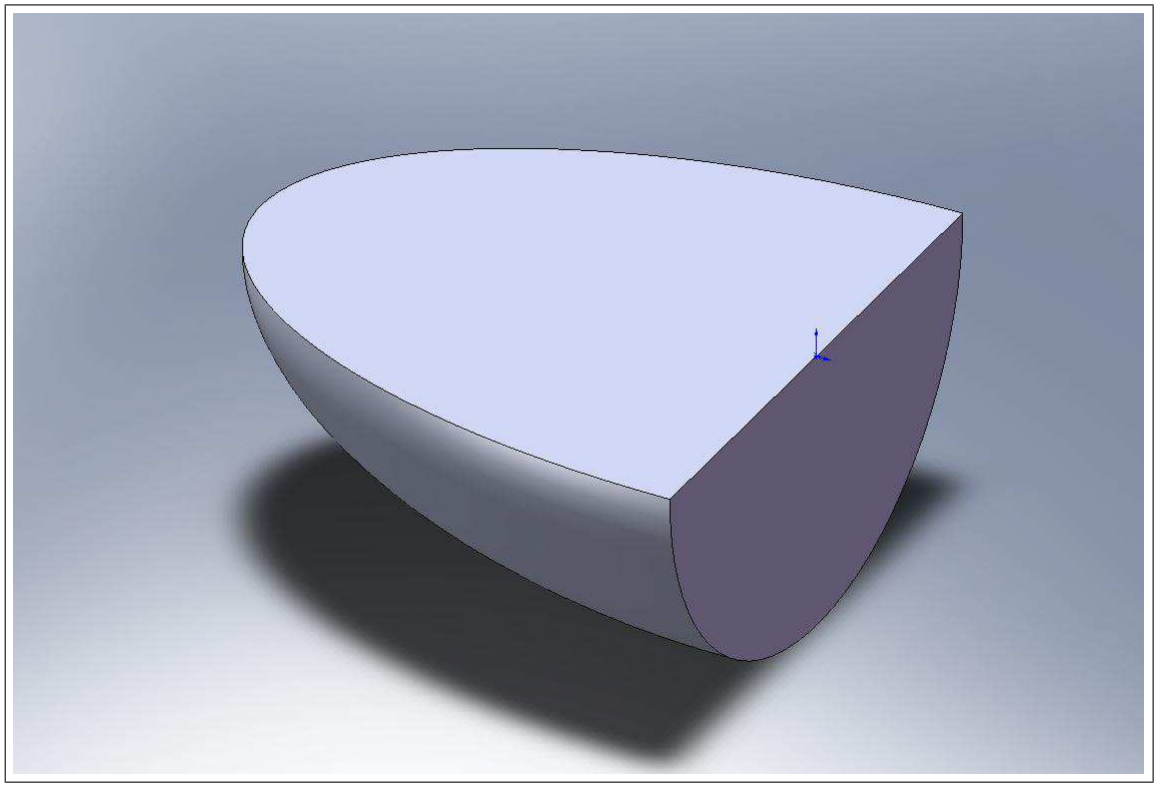

Figure 3.7 A quarter of PC generated in SolidWorks view. It was generated in such a way that any error at the location of the keypoint is not faced.

Material properties and element type were determined using previous studies [3, 4]. For PC a Young's modulus as well as a Poisson's ratio value has been proposed [3, 4]. However, no such value has been proposed for Prony series coefficient or time constant. To resolve this problem, considering skin as the closest tissue to PC, the value of Prony series coefficient and time constant proposed for skin [154] was used for our present PC model. The material properties used were as follows:

- Density: 1 g/cm^3
- Young's Modulus: 0.25×10^6 g/cm^2
- Poisson's Ratio: 0.4
- Shear Elastic Moduli: 0.0864
- Prony Time Constant: 0.212

Subsequently, both the rigid plate and PC were meshed. Meshing process requires optimization. A finer mesh increases accuracy and provides a better contact between the plate and PC; however, it also increases the process time as well as required disc space. The resultant mesh (Figure 3.8) was optimized accordingly.

The other contact surface of circular shape (used for mechanical stimulation; referred to as the *contactor*) was placed parallel to the rigid plate, just above the PC model. Unlike the rigid plate, this surface had no initial contact with the PC. It is because; during some simulations initial contact requires initial penetration setup for the fact that the first node where contact begins is the toughest spot. Digitizing the perfectly smooth surface leads to uncertainty in derivation when calculating the simulation using the numerical method. In such condition, contact may not be established between the contactor and the target elements located on the PC model, which means failure of the simulation. To solve this problem, a certain gap (of 5 μm) was left between the PC model and contactor.

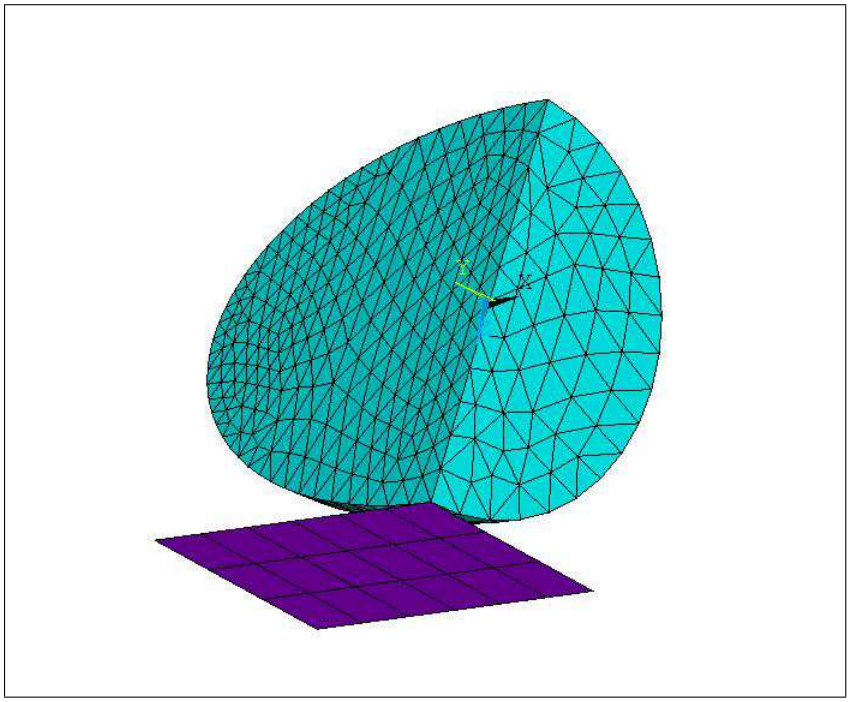

Figure 3.8 Quarter of PC model generated standing on the rigid plate.

The diameter of the contactor used in the actual experiment, was 0.25 mm. The model contactor was modeled in the same dimensions. A fine mesh was used for the contactor (Figure 3.9 and Figure 3.10).

3.2.3 Mechanical Stimulations

The stimulations of both models (i.e., test model and actual PC model) should be considered separately. The test model was set to behave as a high-pass filter with a cut-off frequency of 100 Hz. Sinusoidal stimulations were applied at 10, 50, 80, 100, 160, 200, 250, 500 and 1000 Hz. The stroke length of the stimulations was 0.1 unit considering one side of the cubic model is two units.

The purpose of the stimulations was to mimic the actual experiments. Two types of stimulations were performed:

1. static

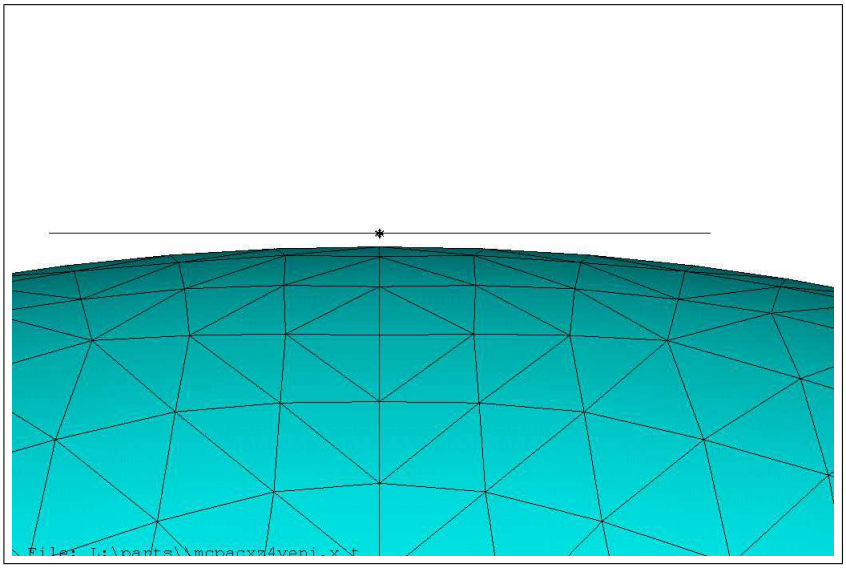

Figure 3.9 The contacting element is placed 5 μm above from the contacting point initially.

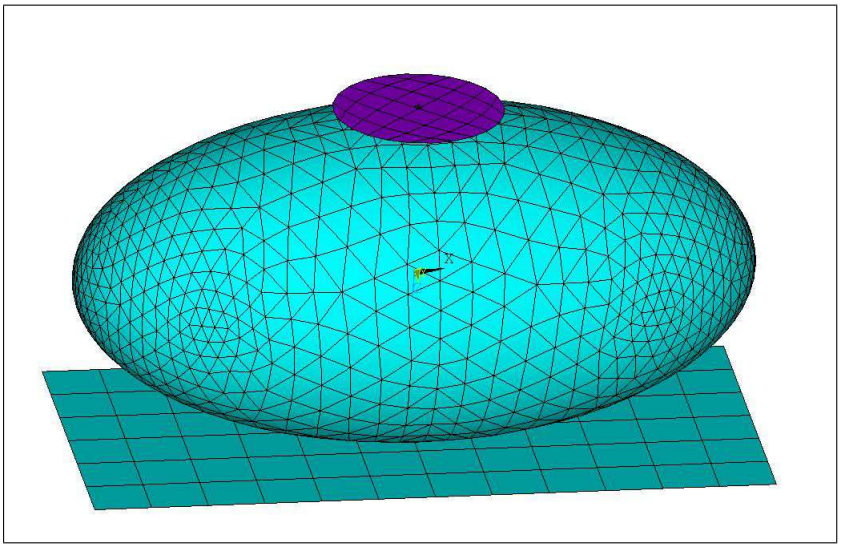

Figure 3.10 The contactor (arranged parallel to the rigid plate) and the PC model.

2. dynamic

In the static simulation, the contactor stimulated the PC by giving ramp compressions. The indentation values of the contactor were the same as the experiments: 10 μm, 20 μm, 30 μm and 40 μm. Note that the contactor moved 5 μm more than indentation values including the gap left.

In the dynamic simulation, the contacting plate performed two subsequent movements:

1. linear displacement of 50 μm for 1 sec.
2. sinusoidal stimulation for 5 cycles on the average.

Sinusoidal stimulations were performed in two different amplitudes (0.05 μm and 20 μm) and several frequencies (1 Hz, 3 Hz, 10 Hz, 32 Hz, 100 Hz, 250 Hz, 320 Hz and 1000 Hz).

4. RESULTS

4.1 Test Model

As it can be seen in Figure 3.3, there are nodes aligned in three different layers. The nodes on the floor layer have zero displacement. The nodes on the ceiling have a sinusoidal displacement. The displacement values in the z-axis direction are identical. Each side of the cube has a length of 2 units while the stroke length is 0.1 units.

The stimulations had 10 periods at each frequency. At the last period, the difference between the minimum and maximum points was recorded. All the measurements were taken from one randomly determined node from the middle layer. It was essential to have a middle layer so that measurements could be performed.

The measurements at each frequency are given in Table 4.1 and plotted in Figure 4.1.

Table 4.1
Results of the test model simulation. The results are represented in units.

	Max (10^{-2})	Min (10^{-2})	P-P Value (10^{-2})
10 Hz	0.412787	-0.412901	0,825688
50 Hz	2.0387	-2.03598	4,07468
80 Hz	2.8216	-2.80916	5,63076
100 Hz	3.18039	-3.1672	6,34759
160 Hz	3.7548	-3.73619	7,49099
200 Hz	3.9383	-3.92253	7,86083
250 Hz	4.06387	-4.04975	8,11362
500 Hz	4.24481	-4.24109	8,4859
1000 Hz	4.27733	-4.28068	8,55801

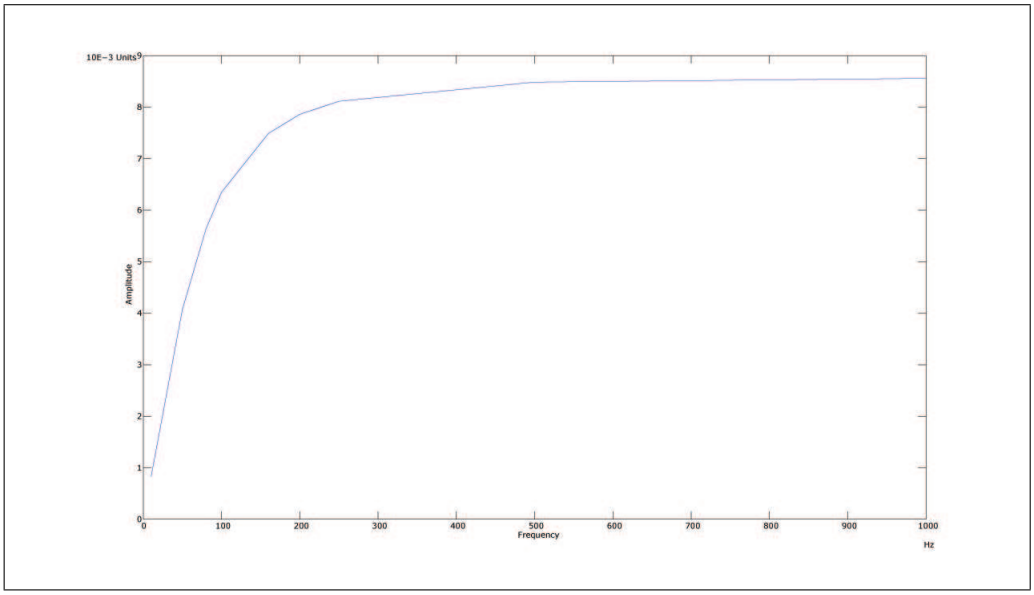

Figure 4.1 The amplitude versus frequency plot (Data from Table 4.1).

4.2 Actual model

4.2.1 Static Indentation Simulation

The actual PC model is first subjected to static indentations. The applied indentations are the same as the ones in the experimental process which are 10 μm, 20 μm, 30 μm and 40 μm of penetration of the contacting probe. These time-free simulations are performed one by one, and as a step function. Thus, steady state solutions are obtained. In Figure 4.2, the x-axis represents normalized values of the z-axis of PC on which the stimulation is applied. Each curve is formed by the simulation of the stated indentation. Nodes on each curve indicate the nodes on the z-axis of the PC, where the stimulation is applied. The distance between adjacent nodes is constant. Thus the values on the x-axis are real displacements of each node after the indentation. The y-axis gives the value of the individual displacement value of each node.

There is another set of data collected after experiments. The collected data has some similarities with the Loewenstein and Skalak's model [2]. Figure 4.3 shows results of both the model in the previous study and the experiment. The curves are obtained after 10 μm indentation of the stimulation probe. X-axis indicates normalized z-axis

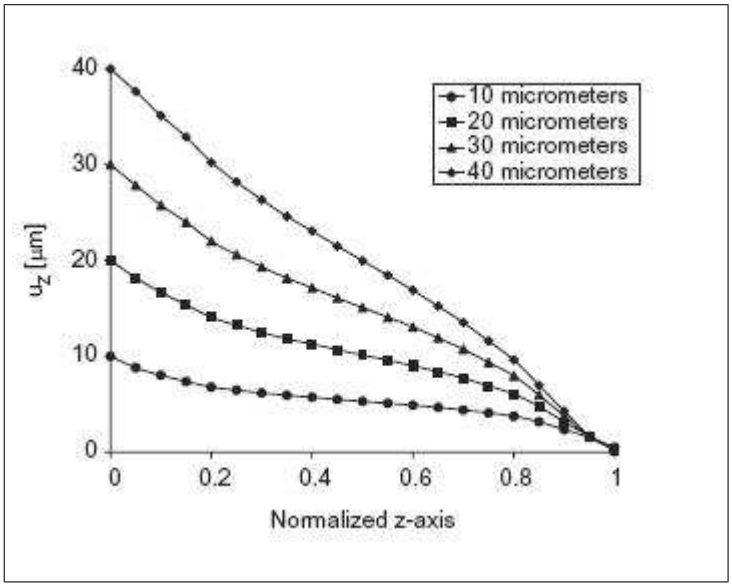

Figure 4.2 Results of finite element model simulation. Each line is formed from the results of different indentation values. Data are collected from 20 equally separated nodes on the stimulation axis [153].

PC length while y-axis gives the real displacement values. The solid line is obtained from the model, and the dash line is obtained from experimental observation.

4.2.2 Dynamic Indentation Simulation

The dynamic stimulations are performed at 1 Hz, 3 Hz, 10 Hz, 32 Hz, 100 Hz, 250 Hz, 320 Hz and 1000 Hz. The time-dependent simulations first have a 50 μm of static indentation. Then sinusoidal displacements are applied at given frequencies with (i) 20 μm and (ii) 0.05 μm amplitudes in the sinusoidal loading region.

The measurements are taken from 2 points on z-axis. One is 125 μm away from the initial contacting point of PC with the stimulator. The other node is 250 μm away which is the center point of PC.

The measurements are taken from the fifth cycle of the simulations. As in the test model, the difference between the minimum and maximum points is measured. The measurements are plotted against frequency. The process is done for both amplitudes.

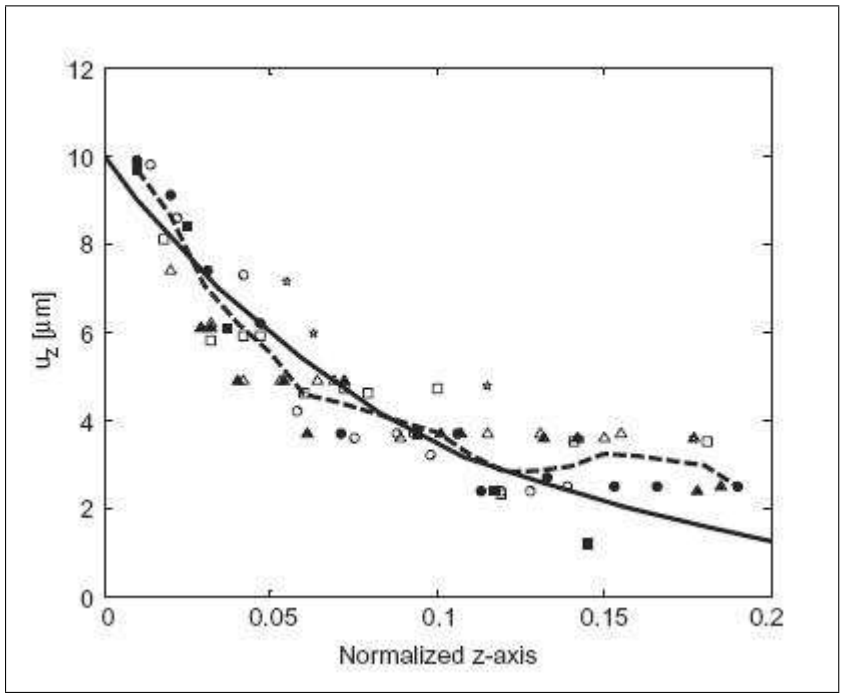

Figure 4.3 Results of Loewenstein and Skalak's model [2] and the performed experiments [153].

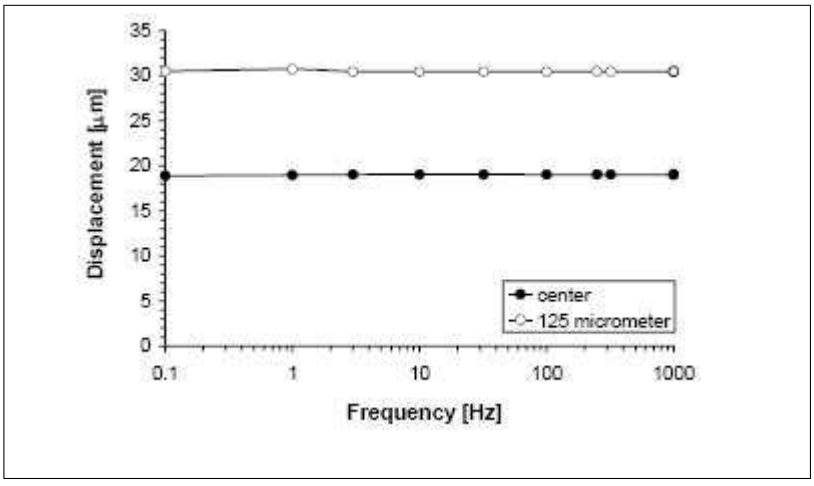

Figure 4.4 Displacement values of center node and the node 125 μm below from the initial contacting node at the corresponding frequencies [153].

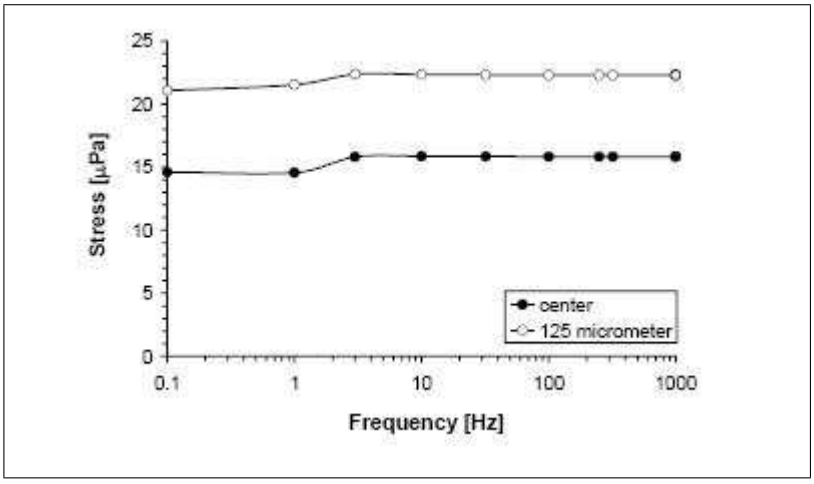

Figure 4.5 Stress values of center node and the node 125 μm below from the initial contacting node of finite element model at the corresponding frequencies [153].

In Figure 4.4 and Figure 4.5, black dots give the results of the nodes at the center, while white dots indicate the nodes equidistant to the center and first contacting node to the stimulator on the z-axis. Data used for drawing the curve for stress versus frequency is obtained in the same way to displacement data, the difference at the peak points of the last cycles are plotted.

The results of the 0.05 μm amplitude of sinusoidal simulations are exactly 400 times smaller than the results of 20 μm amplitude simulations. Hence, those simulations contain no different data than other bigger amplitude simulations. As a result, the shapes of the curves from 0.05 μm amplitude simulations are the same as the curves in Figure 4.4 and Figure 4.5. The only difference is that the values of the y-axis are exactly 400 times smaller.

In Figure 4.6, the node 125 μm away from the center node and first contacting node to the stimulator on the z-axis is plotted. The curve with black dots is drawn with the results of experiments. The curve with white dots indicates the results from finite element model. The experimental data is obtained from the node on the stimulation axis. The node is 100 μm away from the point where stimulation begins. As a close node to the studied node during experiments, the node 125 μm away from center and initial stimulation is accounted. Thus, the curves with black dots are taken from

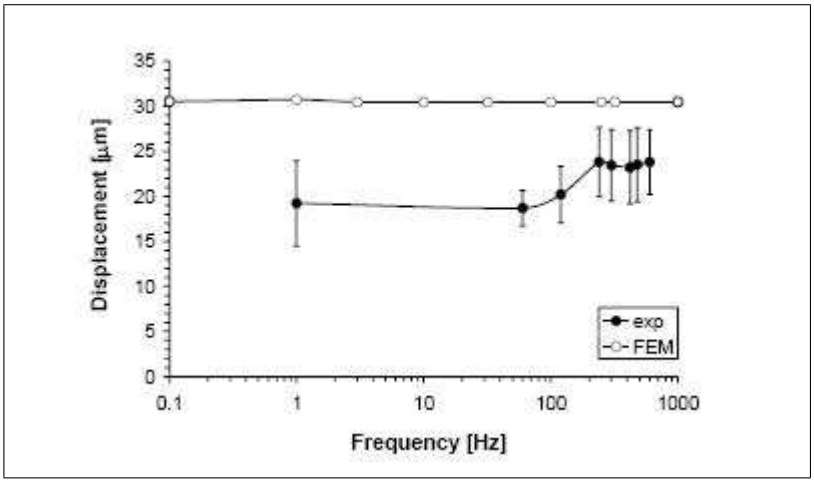

Figure 4.6 Displacement values collected from the node 125 μm below the initial contacting node of finite element model and 100 μm below the same node of the PC in the experiments [153].

the node 100 μm away from stimulation surface; while the curve with white dots is obtained from the node, 125 μm away. The nodes are considered to be close enough to be compared.

5. DISCUSSION AND CONCLUSION

5.1 Test Model

In this study, two models were constructed. The test model was constructed to prove that the actual model is able to provide reliable results. If the model results were the same as predicted, then both models would be able to bring out reliable results.

The test model results should be examined before going through the actual model. The model was constructed to be a Maxwell model which is a characteristic high pass filter model. It was arranged such that when an altering stimulus at a constant stroke length but different frequencies is applied, the stress values at different frequencies within the model vary indicating a manner such as it does not have much stress at lower frequencies but the stress increases with increasing frequency.

This scenario was expected from the test model as well. The test model was posed a number of stimulations with different frequencies. From a constant node at the middle layer, the displacement results were collected after each simulation. The maximum values where the node displaced were derived from results and plotted for corresponding frequencies. The plot can be seen in Figure 4.1. To have an idea, it is essential to give general characteristics of high-pass filter. In Figure 5.1 characteristic high-pass filter curve can be seen.

Another important point to pay attention is that the cut-off frequency is set to be at 100 Hz. The cut-off frequency can be observed in the characteristic high pass filter curve as seen in Figure 5.2. According to the Figure 5.2, the cut-off frequency of the test model can be observed to be at about 100 Hz as expected.

Thus, the results of the model are exactly the same as expected and the manner of the model under sinusoidal stimulation reflected from its setup. This means that

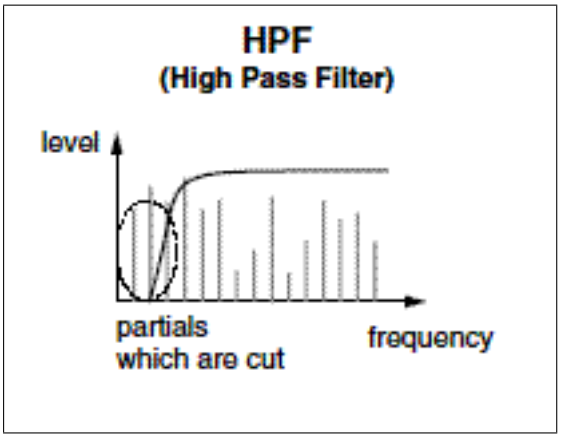

Figure 5.1 Characteristics of a high pass filter. Signals below a certain frequency value can not pass through the filter while higher ones can [Adopted from http://www.roland.com/products/en/_support/ faq.cfm?iCncd=1076&FAQ=EN06-11040&dsp=1&ln=en&prd = SH201].

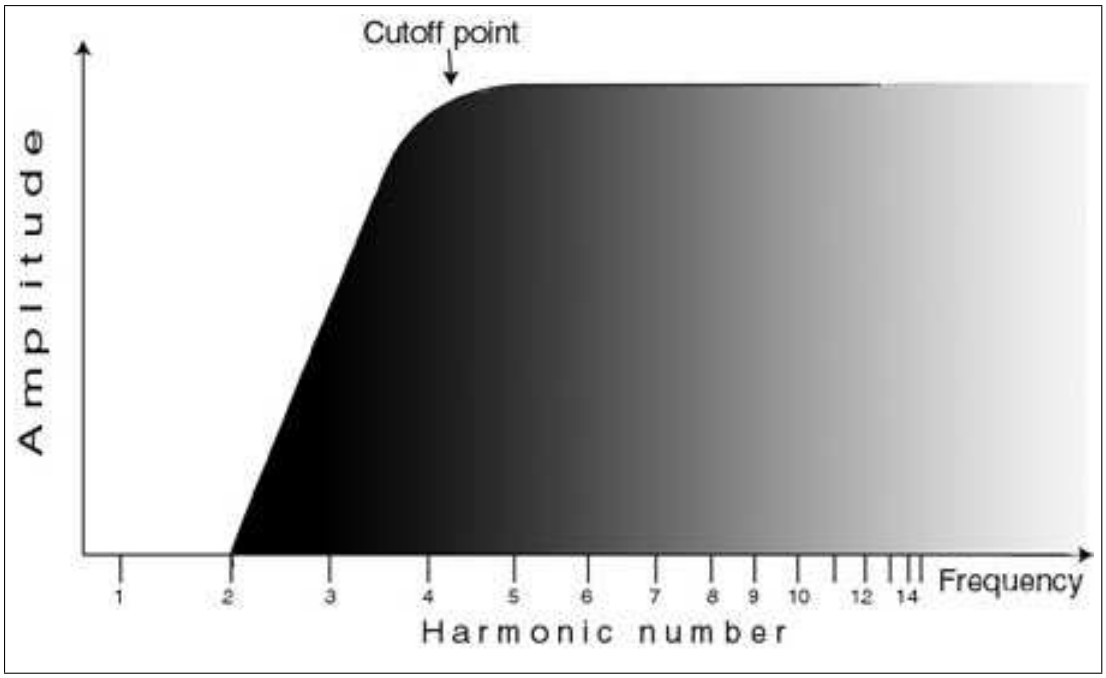

Figure 5.2 The cut-off point which gives the cut-off frequency in the characteristic high-pass filter curve [Adopted from http://www.making-music.com/eq-and-filters_3.html].

the test model and, by implication, the actual model gives reliable results. If the actual model is set up in the way of test model, no other consequences originating from undesired sources will be faced.

5.2 Actual Model

5.2.1 Static Indentation Simulation

In the actual model, two different properties are examined in two different ways. First, the static indentation simulations will be handled. This study is oriented to the first three dimensional finite element model of the PC. Thus, finite element model takes into account the effects of geometry in the calculations. Experimental data did not fit to previous models well [2–4,41]. One of the missing parts of the previous models is that none of them was constructed as a typical PC shape. They were all two-dimensional models. However; three-dimensional geometry of PC may be associating with the static indentation results. The difference between the models and experimental results may be originating from shape of the structures of both subjects.

In the Figure 5.2, the results of the finite element model are presented. The results can be compared with the results of experiments shown in Figure 4.3. As it is clear, during 10 μm indentation application to both model and experiment, for the node that has a normalized value of 0.2 (normalization is: z/width), there is a difference between experimental and model results. The displacement at the experiments is much smaller than the model results. Model results claim that the nodes within the PC yield relatively larger distance.

On the other hand; results of the finite element model have a good agreement with the results of the semi-infinite mathematical PC model [153]. This fact shows that, three-dimensional geometry has no significant effect in mechanical excitation of PC.

It is important to emphasize that the finite element model of PC is constructed assuming that the structure is homogeneous. However, PC has its own characteristic structure of lamellae which may be contributing to its mechanical properties. Considering structural differences of the zones in the PC (explained in details in the introduction section), the mechanical properties of PC varies within itself. Thus, highly complex and layered structure may be a determinant of its mechanical behavior. The decay between the results may not occur if a layered model of PC is proposed.

One of the most important studies on PC was performed by Hubbard [109]. In his studies again a static indentation was applied to PC and displacement of lamellae was measured. His results are not in an agreement with the finite element model results because according to his results the displacement values are not a function of the applied indentation. Instead, the results were non-linear. The difference can be explained by the experiment procedure. In that study, the experiment was recorded from a different angle unlike in the experiments performed in the present study. The camera in Hubbard's experiments [109] was placed on the focal axis as shown in Figure 5.4, perpendicular to the spot where the camera stands in the Figure 3.1. Recording from the same direction of the stimulation may cause an inaccuracy. Another reason for the disparity may be originating from the angle between the plates that compressed the PC as seen in Figure 5.3. The plates, that provided the compression, were attached to each other from one side and between them a PC was placed and stimulations were given. Although there is a correction when comparing the results, it may be an effective difference and may lead uncalculated chain reactions within the PC resulting in nonlinearity. On the contrary, in the simulation described in the methods section, the plates were put to be parallel to each other as in the experiment. Another reason can be put forward is that Hubbard applied very large displacements relatively to the other experiments which might have caused nonlinear results [109]. This may also be an explanation to why the previous experimental study did not give related results to the current experimental study (Figure 5.5).

It should also be noted that the results collected from previous models did not satisfy the results of experimental data and a more convenient model is needed.

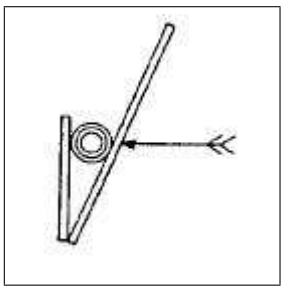

Figure 5.3 In Hubbard's study [109] two flats were used to compress the PC in between and the plates were attached from one side so they had an angle between [109].

Nevertheless, the results of a previous model [2] and the experimental data presented in Figure 4.3 seem to be in a good agreement. The agreement is valid for only relatively lower depths and as the depth increases, the difference becomes more significant. To name the reasons of the decay, the assumptions can be written such as rigid and cylindrical core or the incompressible, viscous fluid filled in the elastic layers or weak elastic connections between lamellae. The decay may also be originating from the measurement errors in the computer analysis of the digitized data. Additionally, some displacements under a limit could not be reported because of the low pixel resolution. However, the fact that the displacement boundary conditions were not specified in the previous model should also be taken into consideration which means the good match of results may be just a coincidence.

5.2.2 Sinusoidal Indentation Simulation

After sinusoidal stimulations at determined frequencies were given as inputs to the finite element model, the displacement and stress results are obtained as shown in Figure 4.4 and Figure 4.5. The viscoelasticity property of the PC model may play the major role in mechanical filtering characteristics of the PC. The mechanical filtering property was proven and shown in previous experimental study [41] as seen in the Figure 5.6.

However, the results of the model do not show a band pass filtering behavior. The most significant ratio is obtained to be 0.1773 dB which is too low to be a filter.

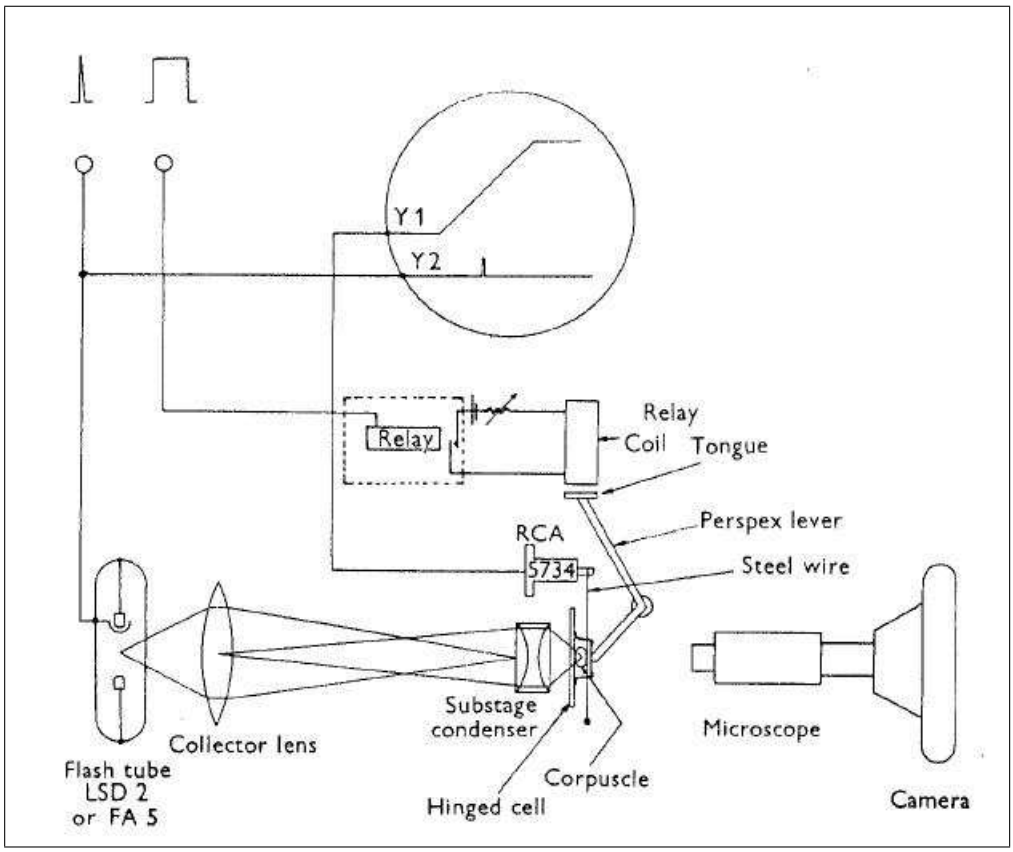

Figure 5.4 The diagram of the apparatus for recording during and after stimulation [109].

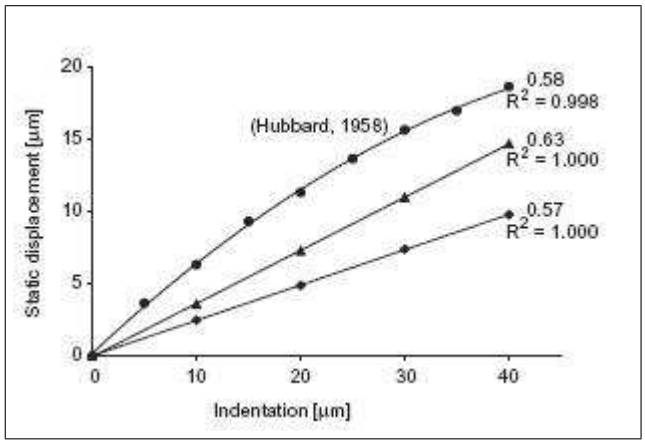

Figure 5.5 The static displacements as a function of the indentation amplitude [153]. Previous data set [109] results with filled circles can be fitted by a parabolic curve, but the current experimental data with triangles and diamonds are linear. Each new experimental curve is derived from different depths. The numbers above the R^2 values indicate the locations of the lamella as the ratios of the radius of the chosen lamella to the radius of the capsule, in Hubbard's [109] reference frame, which has the neurite axis going through the origin.

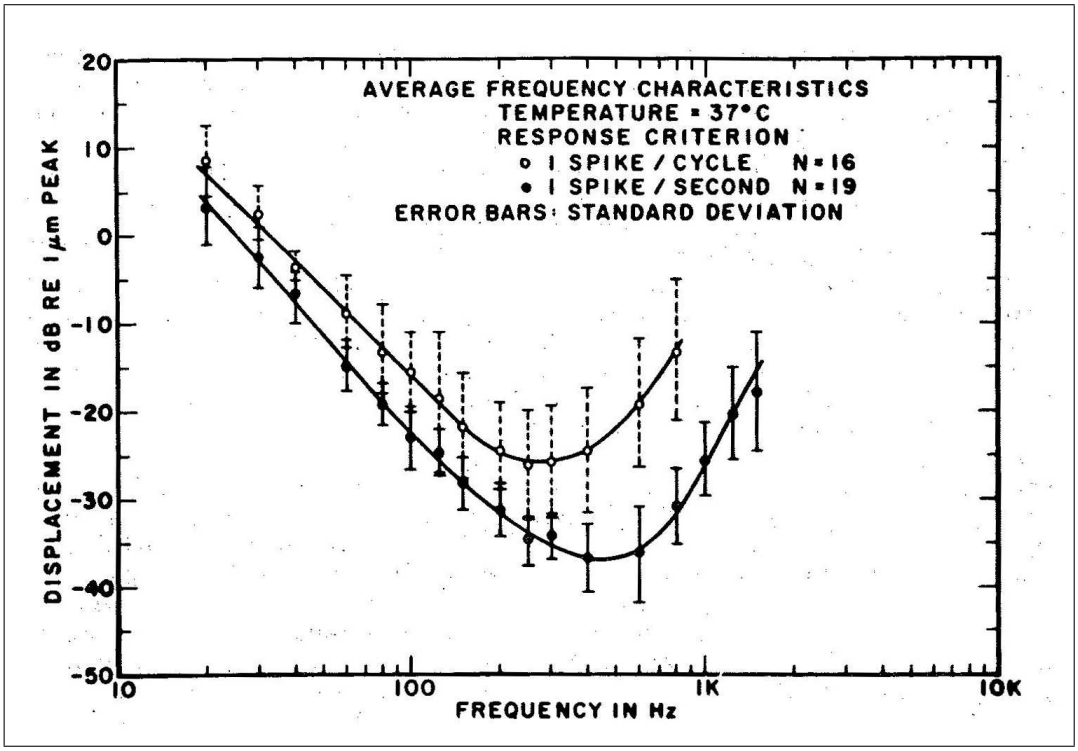

Figure 5.6 The curve was fit through the data by eye and indicates average frequency characteristics for two AP response criteria [41].

Additionally, it was obtained at 0.75 Hz but filtering was expected to be at 250 Hz. It is important to emphasize that viscoelasticity property of PC is not enough to generate a filtering itself.

The discrepancy between results may be because of the homogeneous structure of PC again. Non-homogeneous layered structure with various zone characteristics may probably gain this characteristic property to the PC. It is because in one of the previous model studies [4] the PC was modeled as a multilayer structure. The results of that study illustrated the filtering property clearly (Figure 5.7).

On the other hand, no such filtering property could be observed in the new experimental studies. According to the camera recordings, no mechanical filtering of the PC was observed. The previous experimental study [41] with filtering results shown in Figure 5.6 was obtained only at 0.05 μm amplitude of sinusoidal stimulation. The filtering property was dismissed when the amplitude was 20 μm. Additionally,

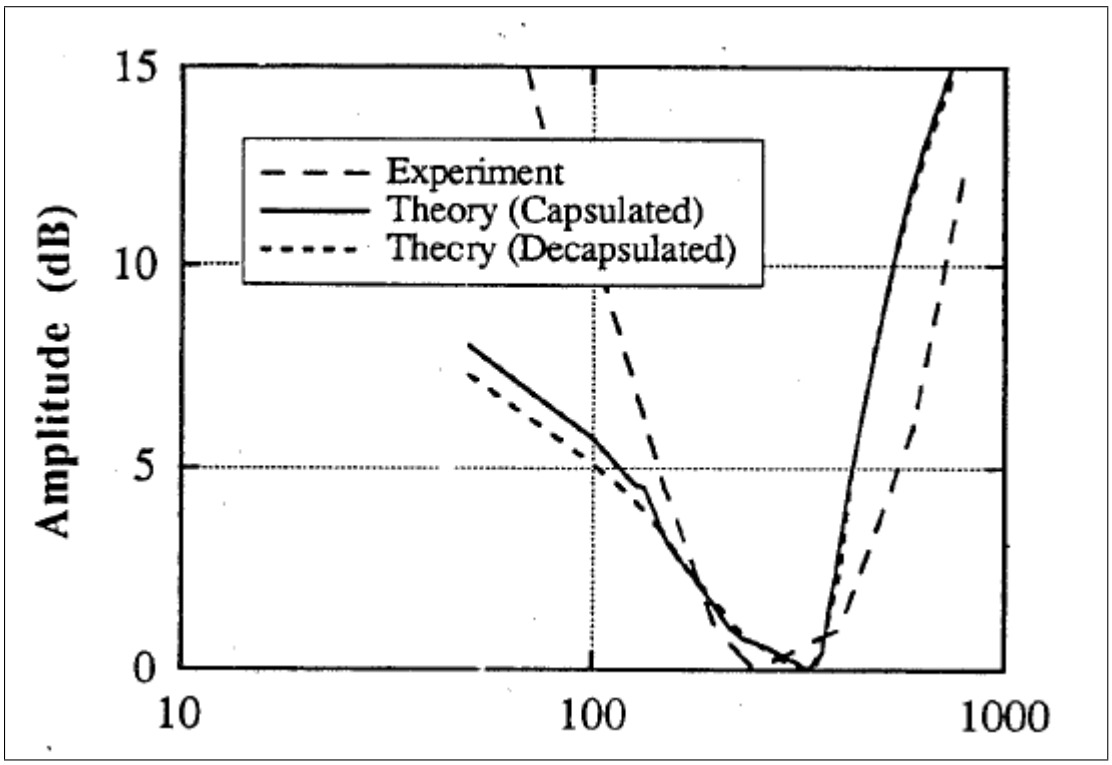

Figure 5.7 The tuning curves were obtained using the criterion of the minimum amplitude produce one spike per cycle for a capsulated and a decapsulated PC [4]. The experimental results were taken from a previous study [26, 27].

the measurements were taken from nerve. New experiments did not contain a sinusoidal stimulation with 0.05 μm amplitude, because of the limited capacity of recording hardware. The camera record could not resolve the displacements within the PC under 0.05 μm amplitude of stimulation. The finite element model was subjected to 0.05 μm amplitude of sinusoidal stimulation, then. However; the results were linear with the indentation amplitude and no filtering property was obtained.

Another interesting point is that; the previous model, from which Figure 4.7 is obtained, consisted of two major components:

1. mechanics of the capsule
2. electrophysiology of the nerve fiber

Consequently, the model [4] with the most relevant results to the experimental

studies, accounted the electrophysiological effects. This fact reveals the idea which claims that the filtering may be associating with the interaction of PC and the nerve innervating it. That may also explain why no such mechanical filtering is obtained in the camera recording experiments and it was obtained only in the experiments where the measurements are taken from the nerve. Such a tuning may be current in Pacinian corpuscles, like in some hearing receptors, as one of the most important and most studied mechanoreceptor [155]. Still no satisfying answer is given with a carefully designed model.

5.3 Future Work

The simulations were repeated with various mechanical properties. However no satisfying quantitative result was obtained. A homogeneous and isotropic model of PC is not enough to explain the PC mechanics. Instead, a more complex model is needed to be constructed. New model should have layers with incompressible fluid in between which will affect the mechanics of the model such that the fluid under a load will increase the compression instead of displacing. More relevant and convincing results can be obtained from such a finite element model. Thus; the original reason of the filtering behavior of the PC can be revealed.

APPENDIX A. ENGINEERING APPLICATIONS OF THE FEM

The finite element method can be used in different branches of engineering applications such as civil engineering, aircraft structure, heat conduction problems, geomechanics, hydrodynamics, hydraulic and water resources engineering, nuclear engineering, biomedical engineering, mechanical design, electrical machines or electromagnetics. For each area there are many examples of different problem types.

In civil engineering structures, the equilibrium problems can be listed as static analysis of trusses, frames, folded plates, shell roofs, shear walls, bridges or prestressed concrete structures. Additionally, natural frequencies, modes of structures or stability of structures are eigenvalue problems of this field and propagation of stress waves, response of structures to aperiodic loads are propagation problems.

In aircraft structures, static analysis of aircraft wings, fuselages, fins, rockets, spacecrafts and missile structures can be considered as the equilibrium problems while natural frequencies, flutter and stability of aircraft, rocket, spacecraft and missile sturectures can be considered as the eigenvalue problems. Response of aircraft structures to random loads, dynamic response of aircraft and spacecraft to aperiodic loads are the propagation problems of this field.

In heat conduction problems, steady-state temperature distribution in solids and fluids can be considered as the equilibrium problems while transient heat flow in rocket nozzles, internal combustion engines, turbine blades, fins and building structures can be considered as the propagation problems.

In geomechanics, analysis of excavations, retaining of wals, undergroung openings, rock joints and soil structure interaction problems; stress analysis in soils, dams, layered piles and machine foundations are the equilibrium problems. Natural frequen-

cies and modes of dam-reservoir systems and soil structure interaction problems are the eigenvalue problems of the same area. Time dependent soil-structure interaction problems, transient seepage in soils and rocks, stress wave propagation in soils and rocks can be considered as the propagation problems in geomechanics.

Analysis of potential flows, free surface flows, boundary layer flows, viscous flows, transonic aerodynamic problems; analysis of hydraulic structures and dams are the equilibrium problems in hydraulic and water resources engineering and hydrodynamics. In these areas, natural periods and modes of shallow basins, lakes and harbors;sloshing of liquids in rigid and flexible containers problems can be considered as the eigenvalue problems and transient seepage in aquifers and porous media; rarefied gas dynamics; magneto-hydrodynamic flows and analysis of unsteady fluid flow and wave propagation problems are the propagation problems.

In nuclear engineering, analysis of nuclear pressure vessels and containment structures; steady-state temperature distribution in reactor components are the equilibrium problems. Natural frequencies and stability of containment structures and neutron flux distribution problem can be considered as eigenvalue problem in nuclear engineering while response of reactor containment structures to dynamic loads, unsteady temperature distribution in reactor components and thermal and viscoelastic analysis of reactor structures problems can be considered as propagation problems.

Stress anaylsis of eyeballs, bones and teeth; load-bearing capacity of implant and prosthetic systems; mechanics of heart valve are the examples of equilibrium problems in biomedical engineering. In biomedical engineering impact analysis of skull or dynamics of anatomical structures can be considered as the propagation problems.

Stress analysis of pressure vessels, pistons, composite materials, linkages and gears or stress concentration problems are the examples of equilibrium problems in mechanical design. Natural frequencies and stability of linkages, gear and machine tools can be considered as the eigen value problems in mechanical design and crack and fracture problems under dynamic loads can be considered as the propagation problems.

In electrical machines and electromagnetics, steady-state analysis of synchronous and induction machines, eddy current and core losses in electric machines and magnetostatics can be considered as the equilibrium problems while transient behavior of electromechanical devices such as motors, actuators or magnetodynamics can be considered as the propagation problems.

REFERENCES

1. Cauna, N., and G. Mannan, "The structure of human digital pacinian corpuscles (corpus cula lamellosa) and its functional significance.," *J Anat*, Vol. 92, pp. 1–20, Jan 1958.

2. Loewenstein, W. R., and R. Skalak, "Mechanical transmission in a pacinian corpuscle. an analysis and a theory.," *J Physiol*, Vol. 182, pp. 346–378, Jan 1966.

3. Holmes, M., and J. Bell, "A model of a sensory mechanoreceptor derived from homogenization," *SIAM Journal on Applied Mathematics*, Vol. 50, pp. 147–166, 1990.

4. Bell, J., and M. Holmes, "Model of the dynamics of receptor potential in a mechanoreceptor.," *Math Biosci*, Vol. 110, pp. 139–174, Jul 1992.

5. Malinovsky, L., *Mechanoreceptors: Development, Structure and Function*, Vol. 34, ch. Classification of sensory nerve endings in vertebrates brought up to date., pp. 261–264. New York: Plenum, 1987.

6. Cauna, N., "Nature and functions of the papillary ridges of the digital skin.," *Anat Rec*, Vol. 119, pp. 449–468, Aug 1954.

7. Cauna, N., *Advances in the Biology of Skin*, ch. The effects of aging on the receptor organs of the human dermis, pp. 63–96. Oxford, Pergamon Press, 1965.

8. Adrian, E. D., and K. Umrath, "The impulse discharge from the pacinian corpuscle.," *J Physiol*, Vol. 68, pp. 139–154, Oct 1929.

9. Loewenstein, W. R., "Biological transducer mechanism," *Biol Bull*, Vol. 121, p. 370, 1961.

10. Loewenstein, W. R., "Facets of a transducer process.," *Cold Spring Harb Symp Quant Biol*, Vol. 30, pp. 29–43, 1965.

11. Gray, J. A. B., and J. L. Malcolm, "The initiation of nerve impulses by mesenteric pacinian corpusels," *Proc R Soc Lond*, Vol. 137, pp. 96–114, 1950.

12. Gray, J. A. B., and P. B. C. Matthews, "Response of pacinian corpuscles in the cat's toe.," *J Physiol*, Vol. 113, pp. 475–482, May 1951.

13. Mendelson, M., and W. R. Loewenstein, "Mechanism of receptor adaptation.," *Science*, Vol. 144, pp. 554–555, May 1964.

14. Iggo, A., and H. Ogawa, "Correlative physiological and morphological studies of rapidly adapting mechanoreceptors in cat's glabrous skin.," *J Physiol*, Vol. 266, pp. 275–296, Apr 1977.

15. Ilyinsky, O. B., and E. I. Komarov, "Effect of beta-irradiation on the bioelectrical activity of a single nerve ending structure (pacini body).," *Radiobiologiia*, Vol. 3, pp. 216–219, 1963.

16. Talbot, R. E., "The effect of beta radiation on mesenteric pacinian corpuscle response," *Radiation Res*, Vol. 42, pp. 539–551, 1970.

17. Ilyinsky, O. B., N. K. Volkova, and V. L. Cherepnov, "Structure and function of the pacinian corpuscles," *Fiziol Zh SSSR Im I M Sechenova*, Vol. 54, pp. 295–302, Mar 1968.

18. Loewenstein, W. R., *Handbook of Sensory Physiology. 1. Principles of receptor Physiology*, ch. Mechano-electric transduction in the Pacinian corpuscle. Initiation of sensory impulses in mechanoreceptor, pp. 269–290. Berlin: Springer, 1971.

19. Scott, D., "Response of pacinian corpuscle to oscillatory stimulation," *Fed Proc*, Vol. 10, p. 123, 1951.

20. Hunt, C. C., and A. K. McIntyre, "Characteristics of responses from receptors from the flexor longus digitorum muscle and the adjoining interosseous region of the cat.," *J Physiol*, Vol. 153, pp. 74–87, Aug 1960.

21. Hunt, C. C., "On the nature of vibration receptors in the hind limb of the cat.," *J Physiol*, Vol. 155, pp. 175–186, Jan 1961.

22. Sato, M., "Response of pacinian corpuscles to sinusoidal vibration.," *J Physiol*, Vol. 159, pp. 391–409, Dec 1961.

23. Talbot, W. H., I. Darian-Smith, H. H. Kornhuber, and V. B. Mountcastle, "The sense of flutter-vibration: comparison of the human capacity with response patterns of mechanoreceptive afferents from the monkey hand.," *J Neurophysiol*, Vol. 31, pp. 301–334, Mar 1968.

24. Bolanowski, S. J., and J. J. Verrillo, "Temperature and criterion effects in a somatosensory subsystem: a neurophysiological and psychophysical study," *J Neurophysiol*, Vol. 48, pp. 836–855, 1982.

25. Bolanowski, S. J., G. A. Gescheider, R. T. Verrillo, and C. M. Checkosky, "Four channels mediate the mechanical aspects of touch.," *J Acoust Soc Am*, Vol. 84, pp. 1680–1694, Nov 1988.

26. Bolanowski, S. J., and J. J. Zwislocki, "Intensity and frequency characteristics of pacinian corpuscles. i. action potentials.," *J Neurophysiol*, Vol. 51, pp. 793–811, Apr 1984.

27. Bolanowski, S. J., and J. J. Zwislocki, "Intensity and frequency characteristics of pacinian corpuscles. ii. receptor potentials.," *J Neurophysiol*, Vol. 51, pp. 812–830, Apr 1984.

28. Verrillo, R. T., "Investigation of some parameters of the cutaneous threshold for vibration," *J Acoust Soc Am*, Vol. 34, pp. 1768–1773, 1962.

29. Lindblom, U., "Properties of touch receptors in distal glabrous skin of the monkey.," *J Neurophysiol*, Vol. 28, pp. 966–985, Sep 1965.

30. Johansson, R. S., U. Landstrom, and R. Lundstrom, "Responses of mechanoreceptive afferent units in the glabrous skin of the human hand to sinusoidal skin displacements.," *Brain Res*, Vol. 244, pp. 17–25, Jul 1982.

31. Vallbo, A. B., and R. S. Johansson, "Properties of cutaneous mechanoreceptors in the human hand related to touch sensation.," *Hum Neurobiol*, Vol. 3, no. 1, pp. 3–14, 1984.

32. Bolanowski, S. J., *Mechanoreceptors: Development, Structure and Function*, ch. Transduction mechanisms in Pacinian corpuscles, pp. 201–207. New York: Plenum, 1988.

33. Montagna, W., and P. F. Parakkal, *The Structure and Function of Skin*, New York: Academic Press, 1974.

34. Aiba, K., "On the sensory innervation of the foot-sole in human adults," *Arch Hist Jap*, Vol. 10, pp. 329–350, 1956.

35. Weddell, G., E. Palmer, and W. Pallie, "Nerve endings in mammalian skin," *Biol Rev*, Vol. 30, pp. 159–193, 1955.

36. Miller, M. R., H. J. Ralston, and M. Kasahara, "The pattern of cutaneous innervations on the human hand," *Am J Anat*, Vol. 102, pp. 183–218, 1958.

37. Bertelli, L., "Sulla presenza di corpuscoli terminali nella parete della'arterioa e della vena poplitea ed in immediata prossimita'a di questi vasi e dei loro collarali," *Atti Accad*, Vol. 21, pp. 250–273, 1953.

38. Lodone, M., "Contributo alla conoscenza dei corpuscoli nervosa terminali situati in diretto raporto od in prossimita dei vasi sanguiferi della gamba. communicazione preliminare," *Monit Zool Ital*, Vol. 62, pp. 490–492, 1953.

39. Cauna, N., and G. Mannan, "Development and postnatal changes of digital pacinian corpuscles (corpuscula lamellosa) in the human hand.," *J Anat*, Vol. 93, pp. 271–286, Jul 1959.

40. Skoglund, C. R., "Properties of pacinian corpuscles of ulnar and tibial locations in cat and fowl," *Acta Physiol Scand*, Vol. 50, pp. 385–386, 1960.

41. Bell, J., S. Bolanowski, and M. H. Holmes, "The structure and function of pacinian corpuscles: a review.," *Prog Neurobiol*, Vol. 42, pp. 79–128, Jan 1994.

42. Quilliam, T. A., *The Somatosensory System*, ch. Some hazards in the interpretation of the pattern of structure in the lamellated receptors, pp. 200–203. MA: Georg Thieme, 1975.

43. Verrillo, R. T., "Comparison of child and adult vibrotactile thresholds," *Bull Psychon Soc*, Vol. 9, pp. 197–200, 1977.

44. Polacek, P., "Differences in the structure and variability of spray-like nerve endings in the joints of some mammals.," *Acta Anat (Basel)*, Vol. 62, no. 4, pp. 568–583, 1965.

45. Beckering, R. E., and J. L. Titus, "Pacinian corpuscles in the adventitia of human femoral-popliteal vessels.," *Arch Pathol*, Vol. 88, p. 204, Aug 1969.

46. Hinsey, J. C., "The innervation of skeletal muscle," *Physiol Rev*, Vol. 14, pp. 514–585, 1934.

47. Shanthaveerappa, T. R., and G. H. Bourne, "New observations on the structure of the pacinian corpuscle and its relation to the perineural epithelium of peripheral nerves.," *Am J Anat*, Vol. 112, pp. 97–109, Jan 1963.

48. Skoglund, S., "Anatomical and physiological studies of knee joint innervation in the cat.," *Acta Physiol Scand Suppl*, Vol. 36, no. 124, pp. 1–101, 1956.

49. Zimny, M. L., and C. S. Wink, "Neuroreceptors in the tissues of the knee joint," *J Electromyo Kinesio*, pp. 148–157, 1991.

50. Shehata, R., "Pacinian corpuscles in bladder wall and outside ureter of the cat.," *Acta Anat (Basel)*, Vol. 77, no. 1, pp. 139–143, 1970.

51. Shehata, R., "Pacinian corpuscles in pelvic urogenital organs and outside abdominal lymph glands of the cat.," *Acta Anat (Basel)*, Vol. 83, no. 1, pp. 127–138, 1972.

52. Shehata, R., "Occasional pacinian corpuscles at the upper part of the cat ureter.," *Acta Anat (Basel)*, Vol. 87, no. 1, pp. 77–81, 1974.

53. Gussen, R., "Pacinian corpuscles in the middle ear.," *J Laryngol Otol*, Vol. 84, pp. 71–76, Jan 1970.

54. Wilson, J. G., "The nerves and nerve endings in the membrane tympani of man," *Am J Anat*, Vol. 11, pp. 101–112, 1911.

55. Kawahara, G., "Studien uber die lamellenkorperchen im pankreas der katze; eine einteilung der lamellenkorperchen," *Arch Hist Jap*, Vol. 3, pp. 189–200, 1952.

56. Takashi, M., I. Sakai, and H. Usizima, "On the terminal neural apparatus detectable in the retroperitoneum of man; a complex pattern of pacinian corpuscle.," *Anat Rec*, Vol. 122, pp. 17–37, May 1955.

57. Roberts, W. H., "Lamellated corpuscles (pacinian) in relation to the larger limb vessels and a comparative study of their distribution in the mesentery," *Anat Rec*, Vol. 133, pp. 593–604, 1959.

58. Genersich, A., "Beitrag zur normalen und pathologischen histologie der menschlichen pacinischen korperchen," *Ref Virch Jahresber*, Vol. 1, p. 64, 1875.

59. Uematsu, K., "Der anatomische nachweis der zentripetalen nervenfasern im n. splanchnicus major," *Acta Scol Medic Univ Imp Kioto*, Vol. 10, pp. 319–323, 1927.

60. Takashi, M., "On the development of the complex pattern of pacinian corpuscle distributed in the human retroperitoneum.," *Anat Rec*, Vol. 128, pp. 665–677, Aug 1957.

61. Shanthaveerappa, T. R., and G. H. Bourne, "Pacinian corpuscle on the olfactory bulb of the squirrel monkey.," *Nature*, Vol. 209, p. 1260, Mar 1966.

62. Pallie, W., K. Nishi, and C. Oura, "The pacinian corpuscle, its vascular supply and the inner core.," *Acta Anat (Basel)*, Vol. 77, no. 4, pp. 508–520, 1970.

63. Hebel, R., and A. Schweiger, "On the fine structure and function of sensory receptors," *Zentralbl Veterinarmed A*, Vol. 14, pp. 15–25, Jan 1967.

64. Kanagasuntheram, R., A. Krishnamurti, W. C. Wong, M. M. Ahmed, and H. L. Chan, "Multiple innervation of the pacinian corpuscle of slow loris–an ultrastructural study.," *Singapore Med J*, Vol. 12, pp. 199–204, Aug 1971.

65. Kanagasuntheram, R., A. Krishnamurti, and W. C. Wong, "The digital pacinian corpuscle of slow loris. observations on the lateral processes of the terminal nerve fiber," *Acta Anat (Basel)*, Vol. 81, pp. 108–112, 1971.

66. Kanagasuntheram, R., A. Krishnamurti, and W. C. Wong, "The digital pacinian corpuscle in the slow loris. observations on the lateral processes of the terminal nerve fibre.," *Acta Anat (Basel)*, Vol. 81, no. 1, pp. 108–112, 1972.

67. Brenowitz, G. L., C. D. Tweedle, and J. I. Johnson, "The development of receptors in the glabrous forepaw skin of pouch young opossums.," *Neuroscience*, Vol. 5, no. 7, pp. 1303–1310, 1980.

68. Andres, K. H., "On the ultrastructure of various mechanoreceptors of higher vertebrates," *Anat Anz*, Vol. 124, no. 5, pp. 551–565, 1969.

69. Botezat, E., "Die apparate des gefuhlssinnes der nackten und behaarten saugetierhaut, mit berucksichtigung des menschen," *Anat Anz*, Vol. 42, pp. 193–250, 1912.

70. Clara, M., "Ueber den bau schnabels der waldschnepfe (scopolax rusticola, l.)," *Zeit f Mikr Anat Forsch*, Vol. 3, pp. 1–108, 1925.

71. Quilliam, T. A., and M. Sato, "The distribution of myelin on nerve fibres from pacinian corpuscles.," *J Physiol*, Vol. 129, pp. 167–176, Jul 1955.

72. Pease, D. C., and T. A. Quilliam, "Electron microscopy of the pacinian corpuscle.," *J Biophys Biochem Cytol*, Vol. 3, pp. 331–342, May 1957.

73. Sakada, S., and T. Sasaki, "Blood-nerve barrier in the vater-pacini corpuscle of cat mesentery.," *Anat Embryol (Berl)*, Vol. 169, no. 3, pp. 237–247, 1984.

74. Santini, M., "Numbers of the pacinian corpuscles of the cat pancreas, mesentery and mesocolon," *Anat Rec*, Vol. 163, p. 322A, 1969.

75. Fabian, G., "Pacinian corpuscles and their relationship to the lymphatic system.," *Lymphology*, Vol. 10, pp. 27–31, Mar 1977.

76. Fabian, G., "The demonstration of the lymphatic pathways of the pacinian corpuscles in the mesojejunum of the cat.," *Lymphology*, Vol. 12, pp. 71–76, Jun 1979.

77. Arndt, R., "Was sind pacinische korperchen?," *Virchows Arch*, Vol. 65, pp. 131–137, 1875.

78. Harris, V., "Note on pacinian corpuscles," *Quart J Microsc Sci*, Vol. 22, pp. 399–400, 1882.

79. Thoma, R., "Ueber die abhangigkeit der bendegewebsneubildung in der arterienintima von den mechanischen bedinguhgen des blutumlaufs. das verhalten der arterien in amputation-ssr mpfen," *Virchows Archiv*, Vol. 95, pp. 294–336, 1884.

80. Askanazy, M., "Vater-pacinische koperchen im stamm des menschlichen nervus tibialis," *Anat Anz*, Vol. 8, pp. 423–425, 1892-1893.

81. Grosser, O., "Zur anatomie und entwicklungsgeschichte des gefasssystems der chiropteren," *Anat. Hefte*, Vol. 17, pp. 203–424, 1901.

82. Michalow, S., "Die struktur der typischen vater-pacinischen korperchen and ihre physiologische bedeutung," *Folia Neurobiol*, Vol. 2, pp. 603–624, 1908.

83. Gammon, G. D., and D. W. Bronk, "The discharge of impulses from pacinian corpuscles in the mesentery and its relation to vascular changes," *Am J Physiol*, Vol. 114, pp. 77–84, 1935.

84. Barbolini, G., F. Tischendorf, and S. B. Curri, "Histology, histochemistry, and function of the human digital arteriovenous anastomoses (hoyer-grosser's organs, masson's glomera). i. the possible relationship with pacinian corpuscles.," *Microvasc Res*, Vol. 3, pp. 142–153, Apr 1971.

85. Barbolini, G., F. Tischendorf, and S. B. Curri, "Histology, histochemistry, and function of the digital arterio-venous anastomoses (hoyer-grossera's organs, massona's glomera). iii pacinian corpuscles regressive changes related to senile involution and severe wasting of the arterio-venous anastomoses," *Biochem Exp Biol*, Vol. 10, pp. 345–354, 1972.

86. Tuttle, R. S., and M. McCleary, "Mesenteric baroreceptors.," *Am J Physiol*, Vol. 229, pp. 1514–1519, Dec 1975.

87. Polacek, P., "Nektere nove pohledy na morfologii sensitivnich nervovych zakonceni," *Lek Zpravy (Hradec Kralove)*, Vol. 16, pp. 9–13, 1971.

88. Halata, Z., "The mechanoreceptors of the mammalian skin ultrastructure and morphological classification.," *Adv Anat Embryol Cell Biol*, Vol. 50, no. 5, pp. 3–77, 1975.

89. Spencer, P. S., and H. H. Schaumburg, "An ultrastructural study of the inner core of the pacinian corpuscle.," *J Neurocytol*, Vol. 2, pp. 217–235, Jun 1973.

90. Ide, C., T. Nitori, and B. L. Munger, "The cytology of human pacinian corpuscles: Evidence for sprouting of the central axon," *Arch Histol Jap*, Vol. 50, pp. 363–383, 1987.

91. Ide, C., Y. Yoshida, S. Hayashi, M. Takashio, and B. L. Munger, "A re-evaluation of the cytology of cat pacinian corpuscles ii. the extreme tip of the axon.," *Cell Tissue Res*, Vol. 253, pp. 95–103, Jul 1988.

92. Chouchkov, H. N., "Ultrastructure of pacinian corpuscles in men and cats.," *Z Mikrosk Anat Forsch*, Vol. 83, no. 1, pp. 17–32, 1971.

93. Nishi, K., C. Oura, and W. Pallie, "Fine structure of pacinian corpuscles in the mesentery of the cat.," *J Cell Biol*, Vol. 43, pp. 539–552, Dec 1969.

94. Loewenstein, W. R., and R. Rathkamp, "Localization of generator structures of electric activity in a pacinian corpuscle.," *Science*, Vol. 127, p. 341, Feb 1958.

95. Loewenstein, W. R., and R. Rathkamp, "The sites for mechano-electric conversion in a pacinian corpuscle.," *J Gen Physiol*, Vol. 41, pp. 1245–1265, Jul 1958.

96. Halata, Z., "The ultrastructure of the sensory nerve endings in the articular capsule of the knee joint of the domestic cat (ruffini corpuscles and pacinian corpuscles).," *J Anat*, Vol. 124, pp. 717–729, Dec 1977.

97. Polacek, P., "On the structural differences of the rows of receptors in the vaginal wall of the cat and their possible functional meaning," *Z Mikrosk Anat Forsch*, Vol. 78, no. 1, pp. 1–34, 1968.

98. Cherepnov, V. L., and N. I. Chadaeva, "Characteristics of soluble proteins of pacinian corpuscles," *Biull Eksp Biol Med*, Vol. 91, pp. 332–334, Mar 1981.

99. Landcastle, J. E., J. E. Savage, N. B. Slepecky, and S. J. Bolanowski, "Immunocytochemical studies on the pacinian corpuscle," *Soc Neurosci Abstr*, Vol. 17, p. 105, 1991.

100. Ilyinsky, O. B., and T. L. Krasnikova, "Changes in ionic composition of pacinian corpuscular fluid with activity.," *Neurosci Behav Physiol*, Vol. 5, no. 4, pp. 297–305, 1972.

101. Ilyinsky, O. B., and T. L. Krasnikova, "Ionic composition of pacinian corpuscle fluid in relation to some characteristics of corpuscular activity.," *Fiziol Zh SSSR Im I M Sechenova*, Vol. 58, pp. 434–442, Mar 1972.

102. Ilyinsky, O. B., G. N. Akoev, T. L. Krasnikova, and S. I. Elman, "K and na ion content in the pacinian corpuscle fluid and its role in the activity of receptors.," *Pflugers Arch*, Vol. 361, pp. 279–285, Feb 1976.

103. Zelena, J., "The effect of long-term denervation on the ultrastructure of pacinian corpuscles in the cat.," *Cell Tissue Res*, Vol. 238, no. 2, pp. 387–394, 1984.

104. Zelena, J., "Multiple axon terminals in reinnervated pacinian corpuscles of adult rat.," *J Neurocytol*, Vol. 13, pp. 665–684, Oct 1984.

105. Ide, C., and K. Tohyama, "Macrophages in pacinian corpuscles.," *Acta Anat (Basel)*, Vol. 121, no. 2, pp. 110–114, 1985.

106. Ide, C., "Role of extracellular matrix in the regeneration of a pacinian corpuscle.," *Brain Res*, Vol. 413, pp. 155–169, Jun 1987.

107. Malinovsky, L., L. Pac, J. A. Vega-Alvarez, and W. Bozilow, "The capsule structure of pacinian corpuscles from the cat mesentery.," *Z Mikrosk Anat Forsch*, Vol. 104, no. 2, pp. 193–201, 1990.

108. Hubbard, S. J., "The mechanical properties of pacinian corpuscles.," *J Physiol*, Vol. 132, p. 23P, May 1956.

109. Hubbard, S. J., "A study of rapid mechanical events in a mechanoreceptor.," *J Physiol*, Vol. 141, pp. 198–218, Apr 1958.

110. Ide, C., and S. Hayashi, "Specializations of plasma membranes in pacinian corpuscles: implications for mechano-electric transduction.," *J Neurocytol*, Vol. 16, pp. 759–773, Dec 1987.

111. Gray, J. A., and M. Sato, "Properties of the receptor potential in pacinian corpuscles.," *J Physiol*, Vol. 122, pp. 610–636, Dec 1953.

112. Alvarez-Buylla, R., and J. R. D. Arellano, "Local responses in pacinian corpuscles.," *Am J Physiol*, Vol. 172, pp. 237–244, Jan 1953.

113. Diamond, J., J. A. Gray, and M. Sato, "The site of initiation of impulses in pacinian corpuscles.," *J Physiol*, Vol. 133, pp. 54–67, Jul 1956.

114. Diamond, J., J. A. Gray, and D. R. Inman, "The depression of the receptor potential in pacinian corpuscles.," *J Physiol*, Vol. 141, pp. 117–131, Apr 1958.

115. Loewenstein, W. R., and S. Cohen, "After-effects of repetitive activity in a nerve ending.," *J Gen Physiol*, Vol. 43, pp. 335–345, Nov 1959.

116. Loewenstein, W. R., and S. Cohen, "Post-tetanic potentiation and depression of generator potential in a single non-myelinated nerve ending.," *J Gen Physiol*, Vol. 43, pp. 347–376, Nov 1959.

117. Loewenstein, W. R., "The generation of electric activity in a nerve ending.," *Ann N Y Acad Sci*, Vol. 81, pp. 367–387, Aug 1959.

118. Polacek, P., and K. Mazanec, "Ultrastructure of mature pacinian corpuscles from mesentery adult cats," *Z. mikro.-anat. Forsch.*, Vol. 75, pp. 343–354, 1966.

119. Munger, B. L., Y. Yoshida, S. Hayashi, T. Osawa, and C. Ide, "A re-evaluation of the cytology of cat pacinian corpuscles. i. the inner core and clefts.," *Cell Tissue Res*, Vol. 253, pp. 83–93, Jul 1988.

120. Chouchkov, C. N., "Ultrastructural differences between the preterminal nerve fibres and their endings in the mechanoreceptors, with special reference to their degeneration and mode of uptake of horseradish peroxidase.," *Prog Brain Res*, Vol. 43, pp. 77–87, 1976.

121. Shanthaveerappa, T. R., and G. H. Bourne, "Perineural epithelium: a new concept of its role in the integrity of the peripheral nervous system.," *Science*, Vol. 154, pp. 1464–1467, Nov 1966.

122. Krause, W., "Die nervenendigung innerhalb der terminalen korperchen," *Z Mikro Anat Forsch*, Vol. 6, pp. 53–136, 1881.

123. Iwanaga, T., T. Fujita, Y. Takahashi, and T. Nakajima, "Meissner's and pacinian corpuscles as studied by immunohistochemistry for s-100 protein, neuron-specific enolase and neurofilament protein.," *Neurosci Lett*, Vol. 31, pp. 117–121, Aug 1982.

124. Dubovy, P., and L. Malinovsky, "A comparison of ultrahistochemical localization of non-specific cholinesterase activity at three axon portions of the sensory nerve endings and in the node of ranvier," *Verh. Anat. Ges.*, Vol. 80, pp. 955–956, 1986.

125. Ilyinsky, O. B., T. L. Krasnikova, G. N. Akoev, and S. I. Elman, "Functional organization of mechanoreceptors.," *Prog Brain Res*, Vol. 43, pp. 195–203, 1976.

126. Dermietzel, R., *Symposium on Mechanoreception*, ch. Freeze-etch studies of the membranes of the Pacinian corpuscle, pp. 99–107. Berlin: Westdeutscher, 1974.

127. Ilyinsky, O. B., B. V. Krylov, and V. L. Cherepnov, "Study of an optimal form of nerve ending of encapsulated tissue mechanoreceptor (pacinian corpuscle)," *Neurophysiologia*, Vol. 9, pp. 423–428, 1976.

128. Munger, B. L., *Handbook of Sensory Physiology. 1. Principles of Receptor Physiology*, ch. Patterns of organization peripheral sensory receptors, pp. 523–556. Berlin: Springer, 1971.

129. Quilliam, T. A., *Unit design and array patterns in receptor organs*, ch. Touch, Heat and Pain, pp. 86–116. Boston: Little, Brown, 1966.

130. Bolanowski, S. J., J. E. Schyuler, and N. B. Slepecky, "Semi-serial electron-micrographic reconstruction of putative transducer sites in pacinian corpuscles.," *Somatosens Mot Res*, Vol. 11, no. 3, pp. 205–218, 1994.

131. Landcastle, J. E., N. B. Slepecky, and S. J. Bolanowski, "Serial electron-micrographic reconstruction of presumed transducer sites in pacinian corpuscles," *Soc Neurosci Abstr*, Vol. 16, p. 702, 1990.

132. Loewenstein, W. R., "Excitation and inactivation in a receptor membrane.," *Ann N Y Acad Sci*, Vol. 94, pp. 510–534, Sep 1961.

133. Munger, B. L., and C. Ide, "The enigma of sensitivity in pacinian corpuscles: a critical review and hypothesis of mechano-electric transduction.," *Neurosci Res*, Vol. 5, pp. 1–15, Oct 1987.

134. Loewenstein, W. R., "Excitation process in a receptor membrane," *Acta Neuroveget*, Vol. 24, pp. 184–207, 1962.

135. Loewenstein, W. R., "Generator processes of repetitive activity in a pacinian corpuscle.," *J Gen Physiol*, Vol. 41, pp. 825–845, Mar 1958.

136. Loewenstein, W. R., "Biological transducers.," *Sci Am*, Vol. 203, pp. 98–108, Aug 1960.

137. Hunt, C. C., and A. Takeuchi, "Responses of the nerve terminal of the pacinian corpuscle.," *J Physiol*, Vol. 160, pp. 1–21, Jan 1962.

138. Loewenstein, W. R., and R. Altamirano-Orrego, "Generation and propagation of impulses during refractoriness in a pacinian corpuscle.," *Nature*, Vol. 181, pp. 124–125, Jan 1958.

139. Loewenstein, W. R., and R. Altamirano-Orrego, "The refractory state of the generator and propagated potentials in a pacinian corpuscle," *J Gen Physiol*, Vol. 41, p. 805, 1958.

140. Ishiko, N., and W. R. Loewenstein, "Electrical output of a receptor membrane.," *Science*, Vol. 130, pp. 1405–1406, Nov 1959.

141. Ozeki, M., and M. Sato, "Initiation of impulses at the non-myelinated nerve terminal in pacinian corpuscles.," *J Physiol*, Vol. 170, pp. 167–185, Jan 1964.

142. Loewenstein, W. R., "Facilitation by previous activity in a pacinian corpuscle.," *J Gen Physiol*, Vol. 41, pp. 847–856, Mar 1958.

143. Loewenstein, W. R., "Spatial summation of electric activity in a non-myelinated nerve ending.," *Nature*, Vol. 183, pp. 1724–1725, Jun 1959.

144. Ilyinsky, O. B., "Processes of excitation and inhibition in single mechanoreceptors (pacinian corpuscles).," *Nature*, Vol. 208, pp. 351–353, Oct 1965.

145. Ilyinsky, O. B., ""on" and "off" responses in mechanoreceptors.," *Fed Proc Transl Suppl*, Vol. 25, no. 6, pp. 948–952, 1966.

146. Sachs, F., and H. Lecar, "Stochastic models for mechanical transduction.," *Biophys J*, Vol. 59, pp. 1143–1145, May 1991.

147. Bell, J., and M. H. Holmes, "A note on modeling mechano-chemical transduction with an application to a skin receptor.," *J Math Biol*, Vol. 32, no. 3, pp. 275–285, 1994.

148. Turner, M. J., R. Clough, H. C. Martin, and L. J. Topp, "Stiffness and deflection analysis of complex structures," *Journal of Aeronautical Sciences*, Vol. 23, pp. 805–824, 1956.

149. Courant, R., "Variational methods for the solution of problems of equilibrium and vibrations," *Bulletin of American Mathematical Society*, Vol. 9, pp. 1–23, 1943.

150. Przemieniecki, J. S., *Theory of Matrix Structural Analysis*, New York: McGraw-Hill, 1968.

151. Zienkiewicz, C., and Y. K. Cheung, *The Finite Element Method in Structural and Continuum Mechanics*, London: McGraw-Hill, 1967.

152. Spencer, A. J. M., *Continuum Mechanics*, New York: Dover, 1992.

153. Güçlü, B., E. A. Schepis, S. Yelke, C. A. Yucesoy, and S. J. Bolanowski, "Ovoid geometry of the pacinian corpuscle is not the determining factor for mechanical excitation.," *Somatosens Mot Res*, Vol. 23, no. 3-4, pp. 119–126, 2006.

154. Wu, J. Z., R. G. Dong, and D. E. Welcome, "Analysis of the point mechanical impedance of fingerpad in vibration.," *Med Eng Phys*, Vol. 28, pp. 816–826, Oct 2006.

155. Bell, A., "Sensors, motors, and tuning in the cochlea: interacting cells could form a surface acoustic wave resonator.," *Bioinspir Biomim*, Vol. 1, pp. 96–101, Sep 2006.

156. Akoev, G. N., N. P. Alekseev, and B. V. Krylov, *Mechanoreceptors, their Functional Organization*, Springer: Berlin, 1988.